Analysis of Various PCF Structures Using Finite Element Method

By

Khushnub Anwar (201416026)

NowrinNowsher (201416052)

Basharat Nahar Islam(201416055)

A thesis submitted in partial fulfillment of the requirements for the degree of

Bachelor of Science

in

Electrical, Electronics and Communication Engineering

Department of Electrical, Electronics and Communication Engineering
Military Institute of Science and Technology (MIST)
Mirpur Cantonment, Dhaka-1216

December 2017

DECLARATION

We, hereby declare that this thesis report has been written based only on the works and results found by us. Materials of the works or research or thesis by other researchers are mentioned by their references. This thesis, neither in or whole nor in part, has been previously submitted for any degree.

Authors

Khushnub Anwar	**201416026**	________________
Nowrin Nowsher	**201416052**	________________
Basharat Nahar Islam	**201416055**	________________

Thesis supervisor

Dr. Md. Shah Alam
Professor
Department of Electrical and Electronic Engineering
Bangladesh University of Engineering and Technology (BUET)
Dhaka - 1205

Dedicated to

Our Beloved Parents.

Abstract

In our thesis we have analyzed different types of PCF namely, hexagonal, rectangular and terahertz photonic crystal fibers by a special method known as the finite element method. Photonic Crystal Fibers are promising novel technology with several possible applications in wave guides, nonlinear optics, fiber lasers, sensory systems, ultra-wide-band transmission, supercontinuum generation, high power delivery, optical amplifiers, and other functional devices. Due to these advantages during the last decade, photonic crystal fibers (PCFs) have been extensively studied for these applications utilizing their unique capabilities such as endless single mode operation, modifiable & anomalous dispersion, large mode area, non-linear effects, solitons propagation, high birefringence, and enhanced or suppressed optical nonlinearity. These unique characteristics come from the fact that optical properties of the guided modes in the core can be easily manipulated by changing the structure of PCF. The H-PCF and R-PCF have frequency located in the communication band region and the THz-PCF has frequency located in the THz region. We have discussed about the structure like how the different model are made of; characteristic properties like dispersion, confinement loss, v parameter; their construction etc. For the construction of these models we have used a special software named Comsol, a brief discussion of which is given in one of the chapters. Alongside the properties and the structure, we have obtained different graphs and values like confinement loss and v parameter in order to explain the properties more easily. We have also shown the dispersion properties and discussed the probability of flattened and zero dispersion wavelengths.

Acknowledgements

The authors would like to thank Dr. Md. Shah Alam for his coordination, patience and advices through the research. This thesis would not have been completed without his kind support and guidance. We would like to express my gratitude and gratefulness for his instructions, continuous encouragement, valuable discussions, and careful review during the period of this research. His perpetual motivation gave the confidence to carry out this work. We are thankful to him for providing all the necessary information, meaningful discussions and proper guidance.

Our sincere gratitude to the authority of MIST for providing with necessary assistance and allowing to use the university's computers and library resources.

We would also like to pay our solemn regards to our family and friends who supported us generously and encouraged us enormously to complete this job.

Last but not the least we are grateful to the Almighty, without his mercy and help, it would not be possible to complete the job properly and in time.

LIST OF ABBREVIATION

SMF	Single-Mode Fiber
MCF	Multi-Core Fiber
SM	Single Mode
MM	Multi-Mode
LED	Light Emitting Diode
EMPs	Electromagnetic Pulses
TIR	Total Internal Reflection
PBG	Photonic Band Gap
FEM	Finite Element Method
DF-PCF	Dispersion Flattened PCF
ESM	Endlessly Single Mode
NA	Numerical Aperture
ISI	Inter Symbol Interference
SNR	Signal-to-Noise Ratio
PML	Perfectly Matched Layer

CONTENTS

LIST OF TABLES

TABLE OF FIGURES

CHAPTER 1

INTRODUCTION

Communication is broadly defined as the transfer of information from one point to another. When the information is conveyed over any distance a communication system is usually required. By superimposing or modulating the information onto an electromagnetic wave which acts as a carrier for the information signal, within a communication system the information transfer is frequently achieved. This modulated carrier is then transmitted to the required destination and the original information signal is obtained by demodulation. Sophisticated techniques have been developed for this process by using electromagnetic carrier waves operating at radio frequencies as well as microwave and millimeter wave frequencies. However, 'Communication' may also be achieved by using an electromagnetic carrier which is selected from the optical range of frequencies.

1.1 Historical development

The use of visible optical carrier waves or light for communication has been prominent for many years. Signal fires, reflecting mirrors and, more recently, signaling lamps have provided successful, if limited, information transfer. Moreover, as early as 1880 Alexander Graham Bell used a light beam to report the transmission of speech. The photo phone was proposed by Bell just four years after the invention of the telephone. It modulated sunlight with a diaphragm giving speech transmission over a distance of 200m. However, though some investigation of optical communication continued in the early part of the twentieth century its use was limited to mobile, low-capacity communication links. This was due to the lack of suitable light sources and the problem that light transmission in the atmosphere is restricted to line of sight and is severely affected by disturbances such as rain, snow, fog, dust and atmospheric turbulence.

Nevertheless, lower frequency and hence longer wavelength electromagnetic waves proved suitable carriers for information transfer in the atmosphere, being less affected by these atmospheric conditions. These electromagnetic carriers can be transmitted over considerable distances but are limited in the amount of information they can convey by their frequencies depending on their wavelengths.

It may also be noted that communication at optical frequencies offers an increase in the potential usable bandwidth by a factor of around 104 over high-frequency microwave transmission. An additional benefit of the use of high carrier frequencies is the general ability of the communication system to concentrate the available power within the transmitted electromagnetic wave. With the invention of the laser, a renewed interest in optical communication was stimulated in the early 1960s. This device provided a powerful coherent light source.

The previously mentioned constraints of light transmission in the atmosphere tended to restrict these systems to short-distance applications. Despite the problems some modest free space optical communication links have been implemented for applications such as the linking of a television camera to a base vehicle and for data links of a few hundred meters between buildings. There is also some interest in optical communication between satellites in outer space.

The invention of the laser instigated a tremendous research effort into the study of optical components to achieve reliable information transfer using a light wave carrier although the uses of the laser for free space optical communication proved somewhat limited. The proposals for optical communication through dielectric waveguides or optical fibers fabricated from glass to avoid degradation of the optical signal by the atmosphere were made almost simultaneously in 1966 by Kao and Hock ham and Warts. Such systems were displayed as a replacement for coaxial cable or carrier transmission systems. Initially the optical fibers exhibited very high attenuation and were not comparable with the coaxial cables they were. There were serious problems involved in jointing the fiber cables in a satisfactory manner to achieve low loss and to enable the process to be performed relatively easily and repeatedly.

1.2 The general system

An optical fiber communication system has a similarity in basic concept to any type of communication system.

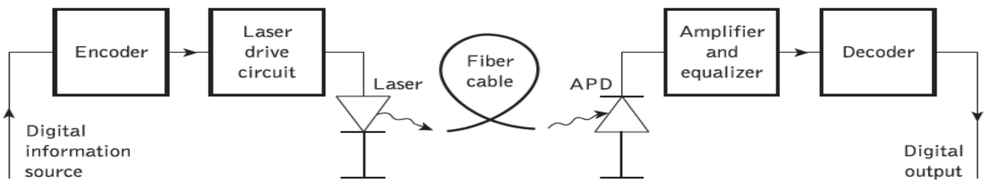

Fig. 1.1**:** A digital optical fiber link using a semiconductor laser source and an Avalanche photodiode (APD) detector.

1.3 Categories of Optical Fiber

Optical fibers fall into two major categories, namely:

- Step index optical fiber
- Graded index optical fiber

1.3.1 Step index optical fiber

Step index optical fiber, which include single mode optical fiber and multimode optical fiber, and graded index optical fiber. Single mode step index optical fiber has core diameter less than 10 micrometers and only allows one light path. Multimode step index optical fiber has a core diameter greater than or equal to 50 micrometers and allows several light paths, this leads to modal dispersion.

1.3.2 Graded index optical fiber

Graded index optical fibers have their core refractive index gradually decrease farther from the center of the core, this increased refraction at the core centre slows the speed of some light rays, thereby allowing all the light rays to reach the receiver at almost the same time, thereby reducing dispersion.

1.4 Various Categories Fiber Mode

According to mode, fibers can be of several types like single mode and multi-mode. Single mode is the fiber containing only one mode and multi-mode is the fiber containing more than one mode.

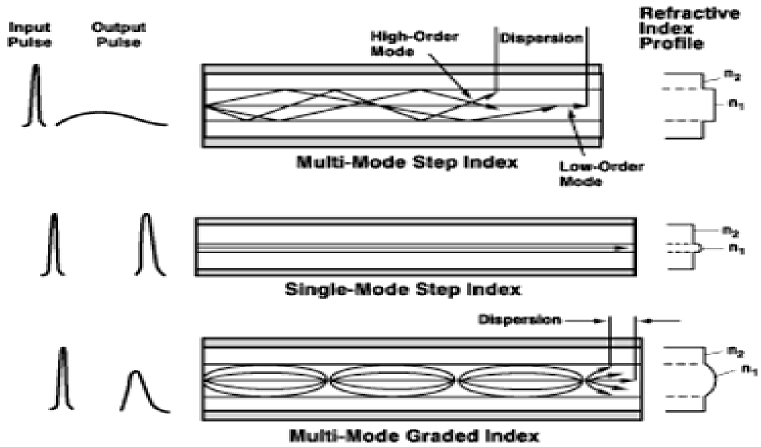

Fig. 1.2: Optical Fiber Modes. (a) Multi-mode step index fiber. (b) Single mode step index fiber. (c) Multi-mode graded index fiber.

In Fig. 1.2 (a) multi-mode step index fiber is shown. In fig 1.2(b) single mode step index fiber is shown and in Fig. 1.2(c) multi-mode graded index fiber is shown.

1.5 Advantages of optical fiber communication

Communication using an optical carrier wave guided along a glass fiber has a number of extremely attractive features which were apparent when the technique was originally conceived. The advances in the technology to date have surpassed even the most optimistic predictions, creating additional advantages. It is useful to consider the merits and special features offered by optical fiber communications over more conventional electrical communications. We commence with the originally foreseen advantages and then consider additional features which have become apparent as the technology has been developed.

This parameter is limited using a single optical carrier signal although the usable fiber bandwidth will be extended further towards the optical carrier frequency. Hence by transmitting several optical signals, each at different center wavelengths, in parallel on the same fiber much enhanced bandwidth utilization for an optical fiber can be achieved. This wavelength division multiplexed operation particularly with dense packing of the optical wavelengths offers the potential for a fiber information-carrying capacity that is many orders of magnitude in excess of that obtained using copper cables [11].

1.6 Objective of the thesis

The objective was to analyze various PCF structures and their properties like H-PCF, R-PCF and THz PCF. The propagation properties of PCF were discussed, and the analysis included determination of PML thickness, fundamental mode, losses and dispersion. In short, we investigated the dependence of the single mode condition and dispersion property for plastic THz PCF.

1.7 Layout of the thesis

In chapter one, we acquainted the readers with the idea of photonic crystal fibers. The general system, the advantages of conventional optical fibers was introduced to distinguish PCF from conventional optical fibers. The motivation and objective of our thesis was also introduced.

Chapter two deals with the properties, construction and the modes on which PCFs operate. We tried to give an extensive idea about the development and application of PCFs. Finally, few popular methods of fabrication of PCFs were stated.

In chapter three, we tried to explain different kinds of dispersion, loss mechanism in PCFs in this chapter. We also gave a short overview of the non-linearity in PCFs and at the end of this chapter V parameter was introduced.

In chapter four, we tried to explain how COMSOL can be used for simulation of analysis on PCF.

From chapter five, it can be found the Analysis of H-PCF, R-PCF and THz PCF was the main focus of this chapter. This chapter also includes the simulations and their results.

Finally, in chapter six, we concluded our work in this chapter and discussed future scopes for our proposed structure.

CHAPTER 2

PHOTONIC CRYSTAL FIBER

Photonic-crystal fiber (PCF) is a new class of optical fiber based on the properties of photonic crystals. Because of its ability to confine light in hollow cores or with confinement characteristics not possible in conventional optical fiber, PCF is now finding applications in fiber-optic communications, fiber lasers, nonlinear devices, high-power transmission, highly sensitive gas sensors, and other areas. More specific categories of PCF include photonic-bandgap fiber (PCFs that confine light by band gap effects), holey fiber (PCFs using air holes in their cross-sections), hole-assisted fiber (PCFs guiding light by a conventional higher-index core modified by the presence of air holes), and Bragg fiber (photonic-bandgap fiber formed by concentric rings of multilayer film). Photonic crystal fibers may be considered a subgroup of a more general class of micro-structured optical fibers, where light is guided by structural modifications, and not only by refractive index differences.

2.1 Modified total internal reflection

It is possible to use a two-dimensional photonic crystal as a fiber cladding, by choosing a core material with a higher refractive index than the cladding effective index. An example of this kind of structures is the PCF with a silica solid core surrounded by a photonic crystal cladding with a triangular lattice of air-holes, shown in Fig. 2.1. These fibers, also known as index-guiding PCFs, guide light through a form of total internal reflection (TIR), called modified TIR. However, they have a number of properties which vary from those of conventional optical fibers.

Fig. 2.1: Triangular lattice solid-core photonic crystal fiber design

2.2 Endlessly single-mode property

As already stated, the first solid-core PCF, shown in Fig. 2.1, which consisted of a triangular lattice of air-holes with a diameter d of about 300 nm and a hole-to-hole spacing Λ of 2.3 μm, did not ever seem to become multi-mode in the experiments, even for short wavelengths. In fact, the guided mode always had a single strong central lobe filling the core [2]. Russell has explained that this endlessly single-mode behavior can be understood by viewing the air-hole lattice as a modal filter or “sieve”.

2.3 Photonic Bandgap Guidance

Optical fiber designs are completely different form the traditional ones that result from the fact that the photonic crystal cladding have gaps in the ranges of the supported modal index β/k where there are no propagating modes. These are the PBGs of the crystal, which are similar to the two-dimensional bandgaps which characterize planar light wave circuits, but in this case, they have propagation with a non-zero value of β. It is important to underline that gaps can appear for values of modal index both greater and smaller than unity, enabling the formation of hollow-core fibers with bandgap material as a cladding,

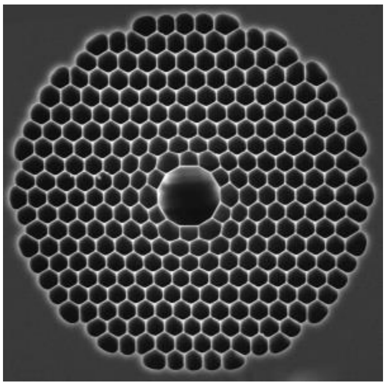

Fig. 2.2: Microscopic picture of a fabricated hollow-core triangular PCF.

as reported in Fig. 2.2. These fibers, which cannot be made using conventional optics, are related to Bragg fibers, since they do not rely on TIR to guide light. In fact, in order to guide light by TIR, it is necessary a lower-index cladding material surrounding the core, but there are no suitable low-loss materials with a refractive index lower than air at optical frequencies. The first PCF which exploited the PBG effect to guide light was reported in 1998, [8]-[10], and it is shown in Fig. 2.3. Notice that its core is formed by an additional air-hole in a honeycomb lattice. This PCF could only guide light in silica, that is in the higher-index material.

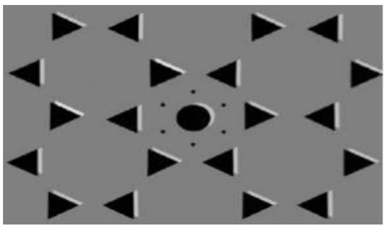

Fig. 2.3: Schematic of the cross-section of the first photonic bandgap PCF with a honeycomb air-hole lattice.

2.4 Solid Core Fibers

Index-guiding PCFs, with a solid glass region within a lattice of air-holes, offer a lot of new opportunities, not only for applications related to fundamental fiber optics. These opportunities are related to some special properties of the photonic crystal cladding, which are due to the large refractive index contrast and the two-dimensional nature of the microstructure, thus affecting the birefringence, the dispersion, the smallest attainable core size, the number of guided modes and the numerical aperture and the birefringence.

2.5 Highly Birefringent Fibers

Where the two orthogonally polarized modes carried in a single-mode fiber propagate at different rates is called birefringent fibers. They are used to maintain polarization states in optical devices and subsystems. The guided modes become birefringent if the core micro structure is deliberately made twofold symmetric, for example, by introducing capillaries with different wall thicknesses above and below the core. By slightly changing the air-hole geometry, it is possible to produce levels of birefringence that exceed the performance of conventional exceed the performance of conventional birefringent fiber by an order of magnitude. It is important to underline that, unlike traditional polarization maintaining fibers, such as bow tie, elliptical-core which contain at least two different glasses, each one with a different thermal expansion coefficient, the birefringence obtainable with PCFs is highly insensitive to temperature, which is an important feature in many applications. An example of the cross-section of a highly birefringent PCF is reported in Fig. 2.4.

2.6 Large mode area fibers

By changing the geometric characteristics of the fiber cross-section, it is possible to design PCFs with completely different properties, that is with large effective area. The typical cross-section of this kind of fibers, called large mode area (LMA) PCFs, consists of a triangular lattice of air-holes where the core is defined by a missing air-hole.

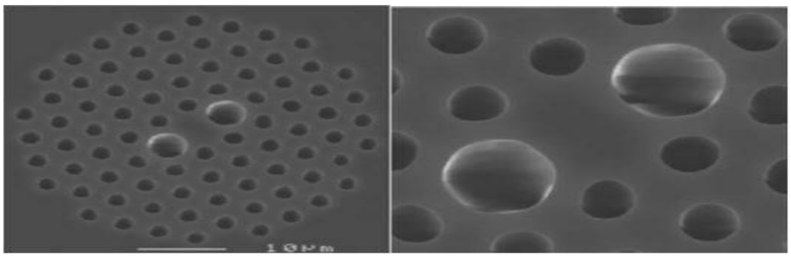

(a) (b)

Fig. 2.4: Microscope picture of (a) the cross-section and (b) the core region of a highly birefringent triangular PCF.

2.7 Modes of operation

Photonic crystal fibers can be divided into two modes of operation, according to their mechanism for confinement. Those with a solid core, or a core with a higher average index than the micro-structured cladding, can operate on the same index-guiding principle as conventional optical fiber — however, they can have a much higher effective refractive index contrast between core and cladding, and therefore can have much stronger confinement for applications in nonlinear optical devices, polarization-maintaining fibers, (or they can also be made with much lower effective index contrast). Alternatively, one can create a "photonic bandgap" fiber, in which the light is confined by a photonic bandgap created by the micro-structured cladding – such a bandgap, properly designed, can confine light in a lower-index core and even a hollow (air) core. Bandgap fibers with hollow cores can potentially circumvent limits imposed by available materials, for example to create fibers that guide light in wavelengths for which transparent materials are not available (because the light is primarily in the air, not in the solid materials). Another potential advantage of a hollow core is that one can dynamically introduce materials into the core, such as a gas that is to be analyzed for the presence of some substance. PCF can also be modified by coating the holes with sol-gels of similar or different index material to enhance its transmittance of light.

2.8 Development of PCF

Year	Development	Applications
1997	Endlessly single mode PCF	A very attractive feature of Endlessly Single Mode PCF is the absence of higher order modes irrespective of the optical wavelength, low loss and low non linearities. These properties are significantly used in mode filtering, sensors, interferometers, etc..
1999	PCF with photonic band gap air core	A different type of wave-guide structure was introduced with additional hole in the center of an array of air holes to be use differently for different applications.
2000	Highly birefringent PCF	PCF made highly birefringent by having different air h diameter along the two orthogonal axes or by asymmetric core design provided high data rates and manufacturing fiber loop mirror.

2000	Super continuum generation in PCF	Super continuum was generated due to PCF's high non-linearity and Zero Dispersion Wavelength find applications in Laser sound Spectroscopy, Pulse Compression, WDM etc..
2001	Fabrication of a Bragg Fiber	Prior to this development manufacturing of fiber and the wrongly field of the fiber Bragg grating were done in two different steps. But in work both fabrication and writing of the Bragg Grating are done single step. Bragg fiber finds extensive application in Optical sensors and fiber lasers.
2001	PCF with double cladding	Ytterbium doped double clad PCF Lasers based on a uniform Fabry Perot configuration provide high power. The cavity was formed between an external high reflecting dichroic mirror at pumped end of fiber.
2002	PCF with ultra-flattened dispersion	Zero Dispersion was obtained at a much wider wavelength range of 1μm -1.6μm used for primarily for supercontinuum generation.
2003	Bragg fiber with silica and air core	This new class of Bragg Fibers reduce non-linearity propagation loss and further serves as a model to study the nonlinear optical phenomenon in gas phase materials.
2004	Chalcogenide Photonic Crystal Fibers(CPCF)	CPCFs offer several distinctive optical properties such as a transmission window that extends far into the infrared spectral region and exhibit an extremely high nonlinear refractive index co-efficient.
2005	Kagome Lattice PCF introduction	Hypo-cycloid shaped Gas filled fiber having three very strong band gap which overlap to provide low loss at a very broad wavelength range by controlling the temperature and pressure of the gas, contribution of gas to the refractive index could be controlled used designing bright spatially coherent optical sources.
2006	Hybrid Photonic Crystal Fiber	This type of PCF composed of air holes and germanium-doped silica rods disposed around an undoes silica core guides light in a core by two mechanisms concurrently which are Total Internal Reflection(TIR)andante resonant reflection.

2007	Silicon Double Inversion on (SDI)Technique for manufacturing Polymer templates for Photonic crystals	The techniques used for manufacturing Polymer Templates couldn't withstand high temperatures required for infiltration. Thus SDI was introduced as an intermediate step where In version silica was made via Atomic Level Deposition (ALD) at room temperature.
2009	Hollow core Photonic Band Fiber free of Surface modes	Due to the elimination of the surface modes, there will be a considerable increase in bandwidth of the fiber and reduce dispersion leading to more carrying capacity.
2013	Double Cladding Seven-core PCF	In double clad Seven core fiber, each core is made to propagate only the fundamental mode called the super mode and provide a great help in creating a Multi core fiber with proper guidance properties for high power super continuum generation.
2014	PCF based Nano displacement sensor	A highly effective Nano-displacement sensor can work for both horizontal as well as vertical displacement. Different sensitivity can be obtained in different displacement regions as requirement.
2015	Design of equiangular spiral Photonic Crystal Fiber	An Equi-angular 8mm long PCF was designed for mid-infrared supercontinuum generation. It could produce large pulses of 500W peak power.
2015	Integration of Photonic Crystal Fibers (PCF) in Fiber Laser	A fully monolithic fiber having 40μm core with Yb doped photonic crystal fiber amplifier module producing up to 210 W average power at 1064 nm was introduced for High Power Applications.

Table 2.1: Development of PCF

2.9 Applications of PCF

Normal conventional optical fiber has so many limitations in its applications, but on the other hand Photonic Crystal Fiber has tremendous applications like [1]-[2]:

i) Sensing Application

   a) Physical Sensors
   b) Curvature/bend Sensors
   c) Displacement/Strain Sensors
   d) Electric and Magnetic Field Sensors

e) Refractive Index Sensors
f) Bio-chemical Sensors
g) Gas Sensors

ii) Medical Applications
a) Medical imaging
b) Nano sensing biomedical instrument

iii) Communication Application

iv) Laser Technology

v) Optical Interconnection

vi) Multi-structured Fiber

2.10 Fabrication technology of PCFs

PCF is a hot topic in the recent age. Designing pure and defectless design is also an important issue. We need to fabricate perfect PCF from design module to achieve our purpose. To do so, there are some efficient ways to follow, [1]-[2].

1. The stack and draw process
2. Extrusion and filling technology
3. Sol-gel technique for fabricating irregular shaped PCF

2.11 Finite Element Method for PCF

At any frequency ω, optical fibers can support a finite number of guided modes whose spatial distribution is a solution of the wave equation,

$$\Delta \times (n^{-1} \times \boldsymbol{H}) - k_o \boldsymbol{H} = 0 \qquad (2.3)$$

called the Hemholtz equation. While the solutions support all the appropriate boundary conditions, the fiber can also support a continuum of unguided radiative modes. In the Hemholtz equation, the optical mode analysis is made on a cross-section in the x-y plane of the fiber. The quantity ***H*** represents the magnetic field and has the form,

$$\boldsymbol{H}(x, y, z, t) = \boldsymbol{H}(x, y) e^{-\boldsymbol{j}(\omega t - \beta z)} \qquad (2.4)$$

Where β is the propagation constant. Equation 2.3 is solved for eigenvalues of the effective index $\lambda = j\beta$. The equation 2.5 is defined for longitudinally-invariant structures composed of nonmagnetic anisotropic materials with diagonal permittivity tensors and e^{jwt} time dependence of the field; it is possible to get a vectoral wave equation expressed only in terms of the transverse components of the magnetic field.

The basic idea of the FEM is that it is a numerical technique which solves the governing equations of a complicated system through a discretization process. The governing

equations can be given in differential form or be expressed in terms of variationally integrals. In FEM, a smooth function is piecewise approximated by means of simple polynomials, each of which is defined over a small region of the domain of the function called element. Instead of expressing the value of the function as a whole, it is expressed in terms of values of the functions at several points (nodes) of the element.
To obtain the nodal field values, the usual Rayleigh-Ritz procedure is employed for the stationary solution of the functions with respect to each of the nodal variables. This can be written in a matrix eigenvalue equation:

$$[A]x - \lambda[B]x = 0 \tag{2.6}$$

Where [A] and [B] are real symmetric matrices, and [B] is also positive definite. The eigenvalue λ may be k_o^2or β^2depedending on the vibrational formulation and x is the eigenvectors representing the unknown nodal field values. It is most desirable for the resulting matrix equation to be of this canonical form, to allow for an efficient and robust solution. This equation 2.6 can be solved by one of various standard subroutines to obtain different eigenvectors and eigenvalues.
There are various types of elements such as one, two and three-dimensional elements available for use in finite element formulations. When the configuration and other details of the problem can be described in terms of two independent spatial coordinates, the two-dimensional elements can be used. Each element is essentially a simple unit within which the unknown can be described in a simple manner. The basic and the simplest element useful for two-dimensional analysis is the triangular element. The smaller the size of the element, the more accurate is the final solution.
By dividing the waveguide cross section into triangular elements, the unknown ***H*** is also considered as to be discretized into corresponding sub-regions. These elements are easier to analyze rather than analyzing the distribution over the whole cross section.

Approximating the fields using quadratic nodal-based basis functions will lead to a sparse generalized matrix eigenvalue equation, which can be solved using an eigenvalue solver to obtain the eigenvalues related to the modal indices (n_{eff}) and eigenvectors associated with the transverse components of the magnetic field $[H_x,Hy]^T$ of the corresponding modes.

CHAPTER 3

PROPERTIES OF PHOTONIC CRYSTAL FIBER

New interpretations of the nature of electric and magnetic fields were developed by Maxwell in the early 1860's. From his equations, the fundamental relationship between electricity and magnetism was realized which stated the changing electric fields create changing magnetic fields and vice versa. This chapter describes Maxwell's field formulation in waveguides. The mode observed in a waveguide is a physical realization of the electromagnetic fields governed by the Maxwell's equations. This description of Maxwell's equations in waveguides serves as the background material for the studies of wave propagation in the fibers that we aim to characterize in our work. For photonic crystals, analytic solutions to Maxwell's equations in such structures are often tedious. With the aid of numerical computation techniques such as the finite-difference frequency domain method, numerical analysis is possible. Waveguide properties are used to characterize the fibers in this thesis, such as the mode type, the origin of the propagation loss, and the dispersion characteristics will also be discussed in detail in this chapter.

3.1 Dispersion Properties

Intermodal dispersion in multimode fibers leads to considerable broadening of short optical pulses (~10ns/km). In the geometrical-optics description, such broadening was attributed to different paths followed by different rays. In the modal description it is related to the different mode indices (or group velocities) associated with different modes.

3.1.1 Group-Velocity Dispersion

Consider a single-mode fiber of length L. A specific spectral component at the frequency ω would arrive at the output end of the fiber after a time delay $T=L/v_g$, where v_g is the group velocity, defined as

$$v_g = \left(\frac{\delta\beta}{\delta\omega}\right)^{-1} \qquad (3.1)$$

The frequency dependence of the group velocity leads to pulse broadening simply because different spectral components of the pulse disperse during propagation and do not arrive simultaneously at the fiber output. If $\Delta\omega$ is the spectral width of the pulse, the extent of pulse broadening for a fiber of length L is governed by

$$\Delta T = \frac{dT}{d\omega}\Delta\omega = \frac{d}{d\omega}\left(\frac{L}{v_g}\right)\Delta\omega = \mathrm{L}\frac{d^2\beta}{d\omega^2}\Delta\omega = \mathrm{L}\beta_2\Delta\omega \qquad (3.2)$$

The dispersion parameter D can vary considerably when the operating wavelength is shifted from 1.3μm. The wavelength dependence of D is governed by the frequency dependence of the mode index. D can be written as

$$D = -\frac{2\pi c}{\lambda^2}\frac{d}{d\omega}\left(\frac{L}{v_g}\right) = -\frac{2\pi}{\lambda^2}\left(2\frac{d\bar{n}}{d\omega} + \omega\frac{d^2\bar{n}}{d\omega^2}\right) \tag{3.3}$$

D can be written as the sum of two terms,

$$D(\lambda) = D_w(\lambda) + D_m(\lambda) \tag{3.4}$$

3.1.2 Material Dispersion

Material dispersion occurs because the refractive index of silica, the material used for fiber fabrication, changes with the optical frequency component. On a fundamental level, the origin of material dispersion is related to the characteristic resonance frequencies at which the material absorbs the electromagnetic radiation. Far from the medium resonances, the refractive index n(λ) is well approximated by the Selmer equation.

$$n^2(\lambda) = 1 + \frac{B_1\lambda^2}{\lambda^2 - C_1} + \frac{B_2\lambda^2}{\lambda^2 - C_2} + \frac{B_3\lambda^2}{\lambda^2 - C_3} \tag{3.5}$$

For silica glass the parameters are found to be B1=0.80686642, B2=0.71815848, B3= 0.85416831, C1= 0.068972606μm, C2= 0.15396605μm, C3 = 11.841931μm.

3.1.3 Waveguide Dispersion

The contribution of waveguide dispersion $D_w(\lambda)$ to the dispersion parameter D is given by

$$D_W = -\frac{2\pi\Delta}{\lambda^2}\left[\frac{n_{2g}^2 d}{n_2\omega}\frac{Vd^2(Vb)}{dV^2} + \frac{dn_{2g}}{d\omega}\frac{d(Vb)}{dV}\right] \tag{3.6}$$

and depends on the V parameter of the fiber. It turns out that $D_w(\lambda)$ is negative in the entire wavelength range 0-1.6μm. On the other hand, Dm(λ) is negative for wavelengths below λ_{ZD} and becomes positive above that.

3.1.4 Chromatic Dispersion

The phenomenon of spreading a short pulse of light as different frequency components of the pulse travel at different velocities is called chromatic dispersion. It is the measurement of dependence of phase velocity and group velocity of light on the optical frequency. This chromatic dispersion, D in [ps/(nm.km)], of a PCFs is easily calculated using the formula given in Eq. 2.22. Where, n_{eff} is refractive index of guided mode, c is velocity of light, λ is wavelength of light.

$$D = -\frac{\lambda}{c}\frac{d^2 Re(n_{eff})}{d\lambda^2} \qquad (3.7)$$

If D is less than zero, then the medium is said to have positive dispersion. If D is greater than zero, the medium has negative dispersion.

3.2 Loss mechanism

The most important factor for any optical fiber technology is loss. Losses in conventional optical fibers have been reduced over the last 30 years, and further improvement is unlikely to be reached. The minimum loss in fused silica, which is around 1550 nm, is slightly less than 0.2 dB/km. This limit is important, since it sets the amplifier spacing in long-haul communications systems, and thus is a major cost of a long-haul transmission system.

The optical loss α_{dB}, measured in dB/km, of PCFs with a sufficiently reduced confinement loss, can be expressed as

$$\alpha_{dB} = \frac{A}{\lambda^4} + B + \alpha_{OH} + \alpha_{IR} \qquad (3.8)$$

Here, A, B, α_{OH} and α_{IR} the Rayleigh scattering coefficient, the imperfection loss, and OH and infrared absorption losses, respectively. At the present time the losses in PCFs are dominated by OH absorption loss and imperfection loss. Losses in hollow-core fibers are limited by the same mechanisms as in conventional fibers and in index-guiding PCFs, that is absorption, Rayleigh scattering, confinement loss, bend loss, and variations in the fiber structure along the length. However, there is the possibility to reduce them below the levels found in conventional optical fibers, since the majority of the light travels in the hollow core, in which scattering and absorption could be very low. There are two types of losses:

i) Confinement loss

ii) Bending loss

3.2.1 Confinement Loss

The leakage loss of solid core PCFs, calculated according to the following formula, quickly decreases when the air-hole ring number or the air-hole diameter increases.

$$Confinementloss = \frac{40\pi}{\ln(10)\lambda}\alpha \quad [dBm] \qquad (3.9)$$

Where α is the imaginary part of the complex effective index. The reduction rate of the confinement loss increases in the same way with these geometric parameters. As expected, the loss decreases with larger Λ values for a fixed d/Λ.

3.2.2 Bending Loss

There are two kinds of bending losses. They are micro bending losses and macro bending losses. In terms of mode theory: the part of mode outside the bend is required to travel faster than that on the inside so that a wave front perpendicular to the direction of propagation is maintained. Hence, part of the mode in the cladding region needs to travel faster than the velocity of light in that medium. Since it is not possible, energy associated with this part of the mode is lost through radiation. This radiation is termed as macro-bending loss. Microscopic meandering of core axis is known as micro-bending. Micro-bending losses can occur due to slight surface imperfections during manufacturing, cabling process or cable installation, during service, due to stress for temperature variation etc. It can cause mode coupling between adjacent modes which in turn cause radiation loss.

3.3 V parameter

In general, to verify the aimlessly single mode operation of a PCF it is needed to parameterize the optical properties of a PCF in terms of v parameter that is characterized by the core radius r, the core index nc and cladding index ncl. Now, the v parameter in the step index fiber is given by:

$$V(\nu) = (2\pi\nu/c) r \sqrt{n_c^2 - n_{cl}^2} \,. \qquad (3.10)$$

However, the equation not being valid for a PCF, r, nc and ncl are not clearly defined in a PCF. This problem is solved by introducing a modified v parameter given by:

$$V_{PCF}(\nu) = (2\pi\nu/c) \Lambda \sqrt{n_{eff.c}^2(\nu) - n_{eff.cl}^2(\nu)} \,, \qquad (3.11)$$

Where, neff.c (v) denotes the effective index of the fundamental mode confined in the plastic core &neff.cl (v) denotes the effective index of the mode which distributes over the cladding with a periodic array of the air holes. The v parameter of a PCF can be simplified as :

$$V_{PCF}(\nu) = k\Lambda \sqrt{n_{eff.c}^2(\nu) - n_{eff.cl}^2(\nu)} = k\Lambda \sin\theta = k_\perp \Lambda \qquad (3.12)$$

Where, k = the free space number=2πv/c. Now, The relation:

$$\sqrt{n_{eff.c}^2(\nu) - n_{eff.cl}^2(\nu)} = \sin\theta \qquad (3.13)$$

is derived by using Snails Law in case of the incidence of critical angle at the interface between the core and the cladding regions and k is the transverse component of the free space wave number. The simplified v parameter is used in finding the cut off frequency of the second order mode. The second order mode needs to have one node and fit into the core region. Thus the transverse wavelength of the lowest second order mode that is the cut off wavelength λcutoff is estimated to be 2p because the core diameter is considered to be about 2p. Therefore, vcutoff is estimated as c/2p. The value of v parameter for the lowest second order mode can be given by:

$$V_{PCF}(\nu_{cutoff}) = k_{\perp}\Lambda = \frac{2\pi\nu_{cutoff}}{c}\Lambda \approx \frac{2\pi}{c}\frac{c}{2\Lambda}\Lambda = \pi \qquad (3.14)$$

3.4 Effective Area

Effective area is the area covered by the light during propagation through PCF. It depends on the shape, wavelength (λ) and effective refractive index. It is a quantity of great importance. It was originally introduced as a measure of non-linearity; a low effective area gives a high density of power needed for non-linear effects to be significant. It is also important in the context of confinement loss, micro-bending loss, macro-bending loss, splicing loss, and numerical aperture. It is also related to spot size. Nonlinear effects occur more efficiently in optical channel than in bulk samples of their constituent materials because the optical field is confined to the small core area over long distances. The confinement of the optical field within the core is achieved by the refractive index profile, which determines the field distribution of the fundamental mode. In general, optical power density is given by the optical power divided by the area over which it is distributed. The field of the fundamental mode of single mode fibers bears little resemblance to the refractive index profile and therefore the area of the doped core region itself does not truly represent the area of the mode field. So effective area,A_{eff} of the mode must be calculated from the field distribution. If the electric field is E and field intensity is I then effective area can be defined as Eq. 3.15.

$$A_{eff} = \frac{(\int |E|^2 dA)^2}{\int |E|^4 dA} = \frac{(\int I dA)^2}{\int I^2 dA} \qquad (3.15)$$

3.5 Numerical aperture

Numerical aperture tells about the light gathering capacity of the fiber. It is defined as a dimensionless number that characterizes the range of angles over which the system can accept or emit light. Fig. 3.2 depicts this phenomenon clearly to us. In this figure $NA = Sin\theta$ as the refractive index of air is 1.

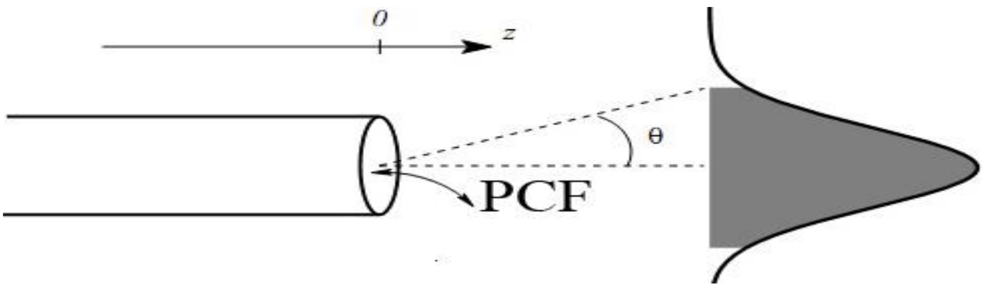

Fig. 3.2: Numerical Aperture (NA) of PCF

In classical optical fiber n_1 and n_2 are the refractive indices of core and cladding respectively. At shorter wavelengths the modal field is tightly confined in silica region, however, at longer wavelengths it penetrates into the air hole which results in reduction of the effective cladding index and hence increase in numerical aperture. So, NA is also related to effective area. For a Gaussian field of width w the standard approximate expression $tan\theta = (\frac{\lambda}{\pi w})$ for the half divergence angle θ of the light radiated from the end-facet of the fiber. The corresponding numerical aperture can then be expressed as Eq. 3.18. Numerical aperture of PCFs increases for large air hole size. We can design PCFs with large numerical aperture by simply controlling its cladding parameters.

$$NA = \sqrt{{n_1}^2 - {n_2}^2} \tag{3.16}$$

$$NA = \sqrt{{n_s}^2 - {n_{cl}}^2} \tag{3.17}$$

$$NA = sin\theta \simeq \left(1 + \frac{\pi A_{eff}}{\lambda^2}\right)^{-\frac{1}{2}} \tag{3.18}$$

3.6 Spot size

It is a measure of extension of electromagnetic field in radial direction. It is very important characteristics of an optical channel as it determines the mode field diameter, splice losses and bending losses. Effective index method has been applied to compute spot size of photonic crystal fibers. It is called mode field radius. So Mode Field Diameter is two times of spot size. The effective area quantifies the transverse extension of the fundamental mode the relation between spot size and effective area is given by Eq 3.19. In PCFs, mode profile gets distorted due to the existence of air-holes pattern arranged in a particular fashion such as triangular for index guided fiber in the cladding region, as a result, mode profile deviates substantially, compared to conventional optical fibers. The far-field intensity distribution of the fundamental mode for an MOF has circular symmetry close to the center, but it becomes hexagonal in the wings of beam. Therefore, we need a suitable definition of spot-size. So to include all this variation two formulas has been given one is for r.m.s spot-size of near-field which is also called Petermann-I spot size of near field and another is for r.m.s spot-size of far field eventually is called Petermann-II spot size of near field. These two formulas have been given by Eq. 3.20 and 3.21 respectively. Spot size as a function of wavelength and air hole size. It is decreased as air hole size is increased and it will increase if wavelength is increased. This is due to the fact that at longer wavelengths the field penetrates into the air holes, reducing the cladding index and hence increasing the refractive index contrast.

$$A_{eff} \quad = \pi w^2 \tag{3.19}$$

$$W_{p1} = \left[\frac{2 \int_0^\infty \psi(r)^2 r^2 r dr}{\int_0^\infty \psi(r)^2 r dr} \right]^{\frac{1}{2}} \tag{3.20}$$

$$W_{p2} = \left[\frac{2 \int_0^\infty \psi(r) r dr}{\int_0^\infty \left(\frac{d\psi}{dr}\right)^2 r dr} \right]^{\frac{1}{2}} \tag{3.21}$$

3.7 Non-Linearity Coefficient

The non-linearity coefficient γ is given by Eq. 3.22, where n_2 is the non-linear index coefficient in the non-linear part of the refractive index. That means $\delta n = n_2 |E|^2$. By knowing n_2 and effective area non-linearity parameter can be determined.

$$\gamma = \frac{n_2 \omega}{c A_{eff}} = \frac{n_2 2\pi}{\lambda A_{eff}} \tag{3.22}$$

Three major nonlinear effects occurring inside optical fiber are self-phase modulation (SPM), cross-phase modulation (XPM), four-wave mixing (FWM) are governed by a single nonlinear parameter γ. For most optical fibers γ has a value of $\sim 1 W^{-1}/km$. It was realized during the 1990s that this value is too small for optical fibers to be useful as a nonlinear medium for practical applications. To solve this problem, several new kinds of fibers with $\gamma > 10 \ W^{-1}/km$ have been developed, and they are collectively referred to as highly nonlinear fibers.

The nonlinear parameter γ can be written as

$$\gamma = \frac{2\pi n_2}{\lambda A_{eff}} = \frac{2\pi \iint_S \ n_2(x,y) I_S^2(x,y) \, dx \, dy}{\lambda \left(\iint_S \ I_S^2(x,y) \, dx \, dy \right)} \tag{3.23}$$

where λ is the wavelength of light and A_{eff} is the effective mode area given in

$$A_{eff} = \frac{\left(\iint_S \ |E_t|^2 \, dx \, dy \right)^2}{|E_t|^4 \, dx \, dy} \tag{3.24}$$

This area depends on the fiber design, and it can be reduced with a proper design to enhance γ. On the other hand, the nonlinear-index coefficient n_2 is a material parameter related to the third-order susceptibility. This parameter is fixed for each glass material. Thus, the only practical approach for enhancing γ for silica-based optical fibers is to reduce the effective mode area A_{eff}. The use of non-silica glasses provides an alternative approach to designing highly nonlinear fibers. Before focusing on the design of such fibers, it is important to discuss the techniques used to determine n_2 experimentally. Accurate measurements of both γ and A_{eff} are necessary for this purpose.

CHAPTER 4

COMSOL FOR PCF

We have used Comsol Multiphysics software of version 4.4.

4.1 Creating a New Model

We can set up a model guided by the Model Wizard or start from a Blank Model.

4.1.1 Creating a model guided by the model wizard

The Model Wizard will guide us in setting up the space dimension, physics, and study type in a few steps:

1. We start by selecting the space dimension for our model component: 3D, 2D Axisymmetric, 2D, 1D Axisymmetric.
2. Now, we add one or more physics interfaces. These are organized in a number of Physics branches in order to make them easy to locate. These branches do not directly correspond to products. When products are added to our COMSOL Multiphysics installation, one or more branches will be populated with additional physics interfaces.
3. We Select the Study type that represents the solver or set of solvers that will be used for the computation. Finally, we click done. The desktop is now displayed with the model tree configured according to the choices we made in the Model Wizard.

4.1.2 Creating a blank model

The Blank Model option will open the COMSOL Desktop interface without any Component or Study. We can right-click the model tree to add a Component of a certain space dimension, physics interface, or Study.

4.2 Parameters, Variables, and scope

4.2.1 Global Parameters

Global parameters are user-defined constant scalars that are usable throughout the model. That is to say, they are “global” in nature. Important uses are:

• Parameterizing geometric dimensions.

• Specifying mesh element sizes.

• Defining parametric sweeps (simulations that are repeated for a variety of different values of a parameter such as a frequency or load).

A global parameter expression can contain numbers, global parameters, built-in constants, built-in functions with global parameter expressions as arguments, and unary and binary operators. For a list of available operators, Language Elements and Reserved Names”. Because these expressions are evaluated before a simulation begins, global parameters may not depend on the time variable t. Likewise, they may not depend on spatial variables like x, y, or z nor on the dependent variables for which our equations are solving. It is important to know that the names of parameters are case sensitive. We define global parameters in the Parameters node in the model tree under Global Definitions.

4.2.2 Geometry

This tutorial uses a geometry that was previously created.

File Locations

The location of the application library that contains the file used in this exercise varies based on the software installation and operating system. In Windows, the file path will be similar to:

C:\Program Files\COMSOL\COMSOL52a\Multiphysics\applications.

In the Model Builder window, under Component 1, right-click Geometry 1 and select Import. As an alternative, we can use the ribbon and click Import from the Geometry tab.

In the Settings window for Import, from the Source list, select COMSOL Multiphysics file.
Click Browse and locate the file wrench.mphbin in the application library folder of the COMSOL installation folder. Its default location in Windows is:

C:\ProgramFiles\COMSOL\COMSOL52a\Multiphysics\applications\COMSOL_Multiphysics\ Structural Mechanics\wrench.mphbin
Double-click to add or click Open.

4.2.3 Materials

The Materials node stores the material properties for all physics and all domains in a Component node. Use the same generic steel material for both the bolt and tool. Here is how to choose it in the Model Builder.

1. Open the Add Materials window. You can open the Add Materials window in either of these two ways:
   -Right-click Component 1 > Materials in the Model Builder and select Add Material
   - From the ribbon, select the Home tab and then click Add Material.
2. In the Add Material window, click to expand the Built-In folder. Scroll down to find Structural steel, right-click, and select Add to Component 1.
3. Examine the Material Contents section in the Settings window for Material to see the properties that are available. Properties with green check marks are used by the physics in the simulation.
4. Close the Add Material window.

4.3 Selecting Boundaries and Other Geometric Entities

When a boundary is unselected, its color is typically gray, the exception being when we use the material Appearance setting available in Materials; To select a boundary, first hover over it. This highlights the boundary in red, assuming the boundary was previously unselected. Now, click to select the boundary by using the left mouse button. The boundary now turns blue. Its boundary number will appear in the Selection list in the Settings window of the corresponding boundary condition. Once a boundary is selected and you hover over it again, the boundary turns green. If you click a boundary highlighted in green, the boundary is deselected and now turns gray again. The same technique for selecting and deselecting is applicable to geometry objects, domains, boundaries, edges, and points.

4.3.1 Mesh

The mesh settings determine the resolution of the finite element mesh used to discretize the model. The finite element method divides the model into small elements of geometrically simple shapes, in this case tetrahedrons. In each tetrahedron, a set of polynomial functions is used to approximate the structural displacement field — how much the object deforms in each of the three coordinate directions

In this example, because the geometry contains small edges and faces, we will define a slightly finer mesh than the default setting suggests. This will better resolve the variations of the stress field and give a more accurate result. Refining the mesh size to improve computational accuracy always involves some sacrifice in speed and typically requires increased memory usage.

4.3.2 Study

In the beginning of setting up the model, we selected a Stationary study, which implies that a stationary solver will be used. For this to be applicable, the assumption is that the load, deformation, and stress do not vary in time. To start the solver:

- Right-click Study 1 and select Compute (or press F8). After a few seconds of computation time, the default plot is displayed in the Graphics window. We can find other useful information about the computation in the Messages and Log windows; Click the Messages and Log tabs under the Graphics window to see the kind of information available to you. The Messages window can also be opened from the Windows drop-down list in the Home tab of the ribbon.

CHAPTER 5

ANALYSIS OF PCF

Photonic crystal fibers have many unusual properties like endless single mode operation, flexible controlled dispersion properties and high nonlinearity for which they are very attractive from scientific and technological point of view.

For fabricating the PCF normally silica materials are used and its loss is quite high at terahertz frequencies. Polyethylene and polytetrafluorethylene like plastic materials are also found to be transparent in the THz range. Plastic PCFs with a triangular lattice have been recently proposed by Han et al. and Masahiro. They investigated the THz pulse propagation in PCFs and fabrication methods of plastic PCFs. The propagation loss of the plastic THz PCF is dependent upon the field confinement and material absorption.

5.1 Hexagonal Lattice PCF (H-PCF)

H-PCF means hexagonal PCF. That is the shape of the PCF is hexagonal. The range of frequency of this PCF is in communication bands.

5.1.1 Parameters

After initial setup in parameter box parameter is defined. For our purpose we defined pitch, d/A, then we determined d then other parameter was determined to draw the PCF in COMSOL easily.

5.1.2 Geometry of PCF

As mentioned earlier we simulated hexagonal PCF. So, to simulate this we first draw the PCF. To draw this at first a large circle is drawn, then many small circles are drawn with the given parameter in line, the space between two air holes is equal to pitch and the radius of air hole is determined from d/Λ ratio. The center of each air hole is determined from pitch and by applying the formula of equilateral triangle. After drawing all circles center air hole is removed to make the fiber index guided. Then a large circle is again drawn. The difference of radius between this large circle and previous large circle is the thickness of PML. Finally, the figure will look like Fig. 5.1.

5.1.3 Material Selection

After drawing geometry next step is to specify proper material for each part from material section. In air hole we used air as material and the refractive index of air is given.

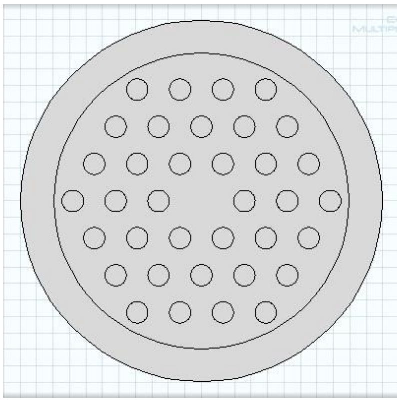

Fig. 5.1: Hexagonal PCF for pitch 2.6 $\boldsymbol{\mu m}$ in COMSOL

5.1.4 Refractive index

The refractive index of air is given which is 1. Then for first big circle we used silica as a material. The refractive index of silica is a function of wavelength.

$$n^2(\lambda) = 1 + \frac{B_1\lambda^2}{\lambda^2 - C_1} + \frac{B_2\lambda^2}{\lambda^2 - C_2} + \frac{B_3\lambda^2}{\lambda^2 - C_3} \qquad (5.1)$$

This dependency equation is known as Selmer equation. Here value of B_1 is 0.6961663, B_2 is 0.4079426, B_3 is 0.8974794, C_1 is 0.0047, C_2 is 0.0135 and C_3 is 97.9340. By plotting this equation in MATLAB we got the Fig. 5.2.

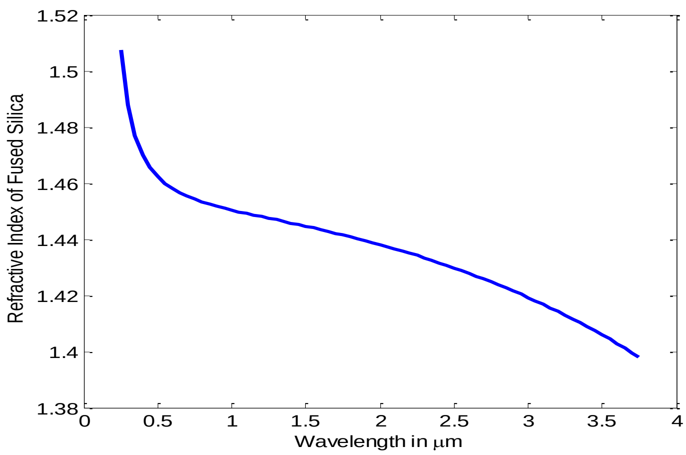

Fig.5.2: Refractive Index of Silica

Now for operating wavelength at 1.55 μm the value of refractive index is 1.444. So, to find the fundamental mode in normal situation at 1.55 μm we used refractive index as 1.444. But while determining the variation of confinement loss with respect to wavelength then this Selmer equation has been used as refractive index to include the change of refractive index with wavelength. In this case refractive index is a function of wavelength. For each simulation, refractive index was changed by Selmer equation.

5.1.5 Physics and study

After providing refractive index for each part correctly then information about physics is given. Wave equation for refractive index is chosen. Then PML layer is directed to act as PML layer. For PML cylindrical geometry type has been chosen. Then mesh is done. Quality of mesh below coarse mesh may give wrong analysis.

Now all work has been done except study. For simple analysis in Mode analysis box wavelength is given. The mode is usually searched around the highest value of refractive index. Desired number of modes usually varies from 20 to 50. If we need to do same analysis more than one time for example in case of determining relationship with bending loss and bending radius or confinement loss and wavelength parametric sweep can be used. By sweeping correct parameter wavelength for confinement loss and bending radius for bending loss we will get proper result too quickly.

5.1.6 Determining PML thickness

As stated above the thickness of PML is determined by varying this PML thickness and then measuring the complex value of refractive index. A stable imaginary value of refractive index indicates appropriate PML thickness. To find this appropriate thickness in COMSOL at first PML thickness is swept in COMSOL then the effective index is recorded. Then we plot imaginary part of effective index and PML thickness that has been generated by MATLAB. Then plot has been given in Fig. 5.3. From this figure PML thickness from 1 to 3 μm can be used as imaginary part which is stable in this region. So we used PML thickness 2 μm for our simulation as it is in the middle of 1& 3μm.

5.1.7 Determining fundamental mode

Refractive index of silica is used is 1.444 at wavelength 1.55μm. The refractive index of air is used as 1. The wavelength is 1.55μm. By following this procedure we found a fundamental mode of PCF. The field distribution has been given Fig. 5.4. From these field distributions it is very clear to us that in a fundamental mode all power is confined in the core region, so all field are confined in core region. The z component of electric field and magnetic field are perpendicular to each other. The phenomena of power flow and direction of electric and magnetic field has been depicted in Fig. 5.4. By closely looking at the z component of electric or magnetic field we can easily find the way of propagation of light in z direction. The Fig. 5.4 depicts that the light propagates in the z direction periodically. PCF has another fundamental mode. For this mode electric and magnetic field are perpendicular to each other. The field of previous fundamental mode is perpendicular to the field of new fundamental mode. That means the electric field of both modes is perpendicular to each other. Fig. 5.4 depicts these fields for pitch of 2.6μm**.** The effective area for these two modes is 9.898178 μm^2 and 9.897844μm^2 respectively.

The effective area has been determined by the following procedure. At first integration over total surface is done for$(abs(normE))^2$ and(abs(normE)) ^{4}. Then the square of the first result is divided by the second result. This result is effective area as previous formula suggest.

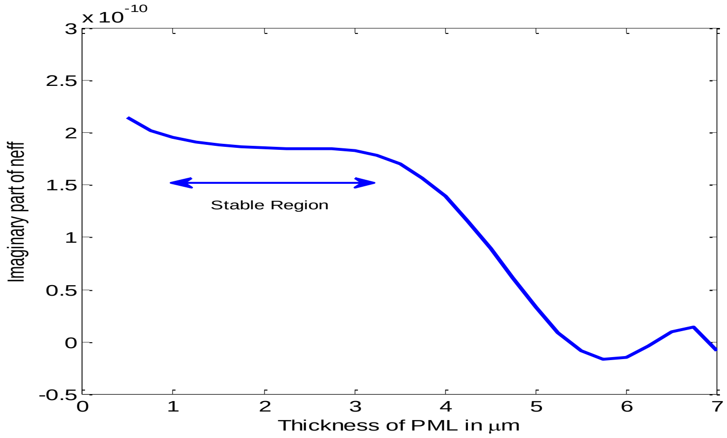

Fig 5.3: Imaginary part of effective index with respect to PML thickness.

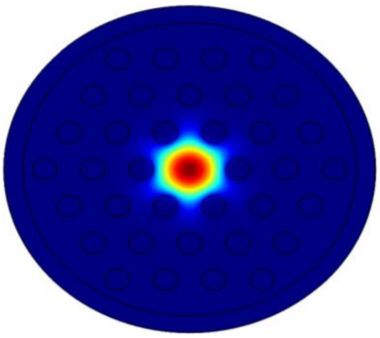

(a) Norm E

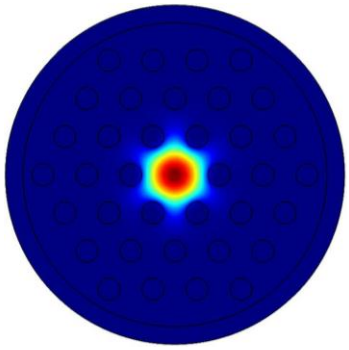

(b) Norm H

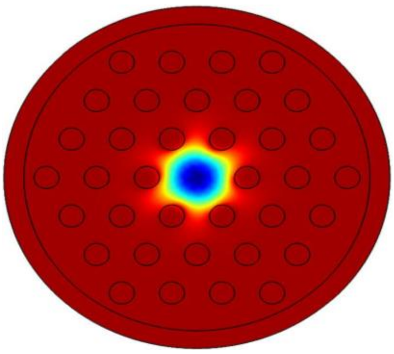

(c) Ex

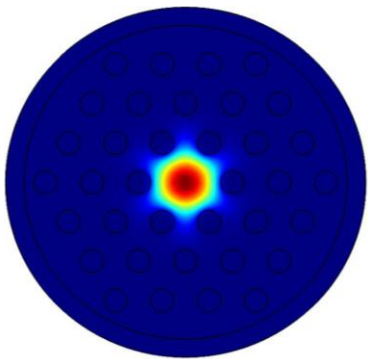

(d) Hx

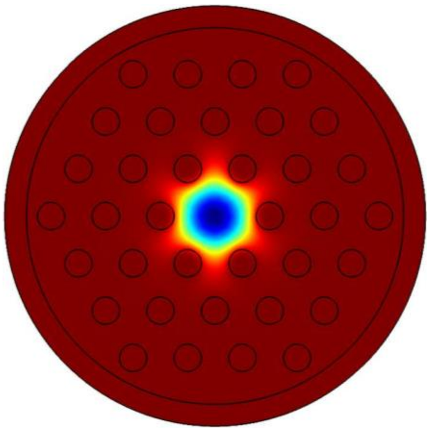

(e) Ey

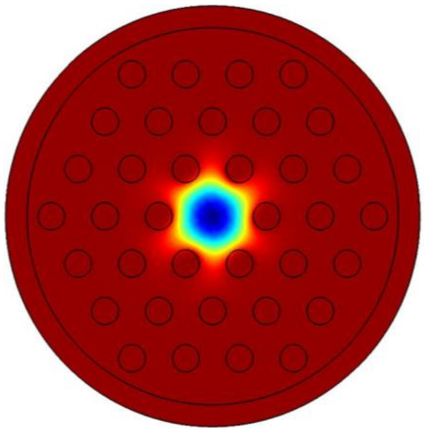

(f) Hy

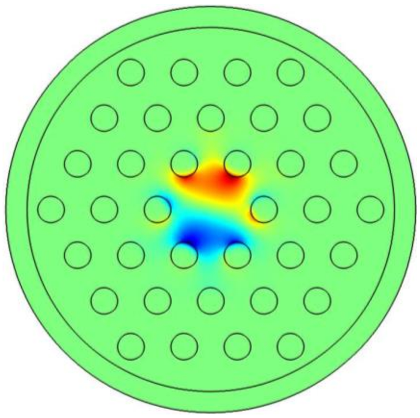

(g) Ez

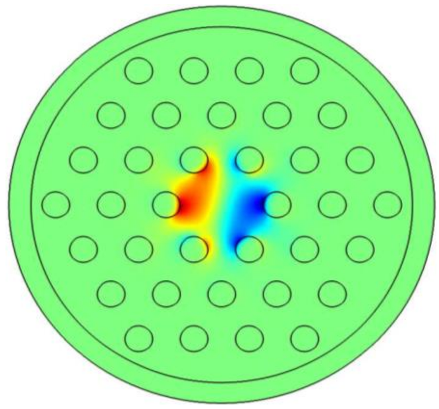

(h) Hz

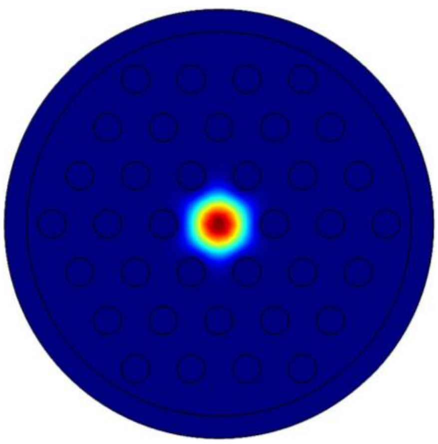

(i)Power flow in z direction

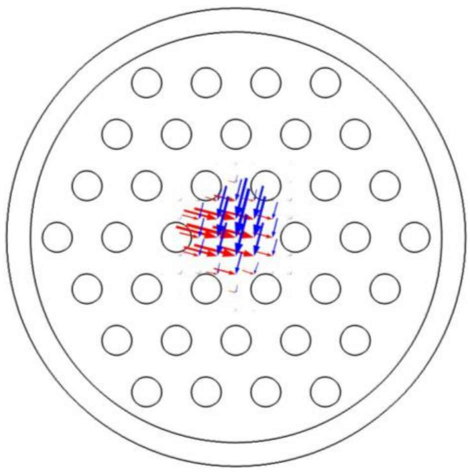

(j) Direction of E and H

Fig. 5.4: Field distribution and power of fundamental mode of H-PCF.

5.1.8Impact of pitch on fundamental mode

For pitch value of 5, 2.6 and 1.6 μm we have simulated the fibers to find fundamental mode. Then we find the fundamental mode for each pitch. This simulation has been done at 1.55μm. The field distribution and effective area is given in fig. 5.5. From field distribution it is obvious to us that for all pitch fundamental mode is confined to the core. No difference can be observed by merely looking these figures. But by looking through effective index and effective area we will get too much difference between them.

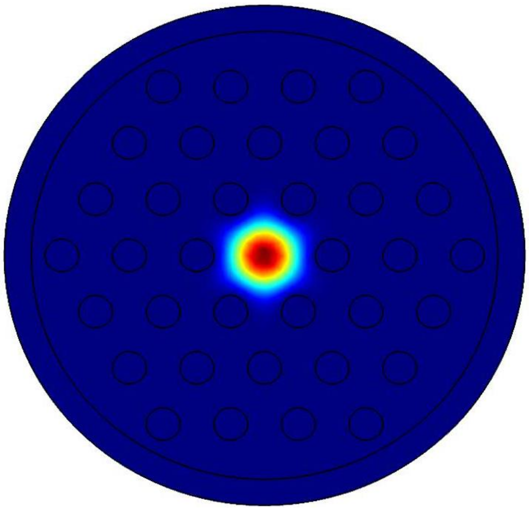

(a) Pz for Λ=5μm

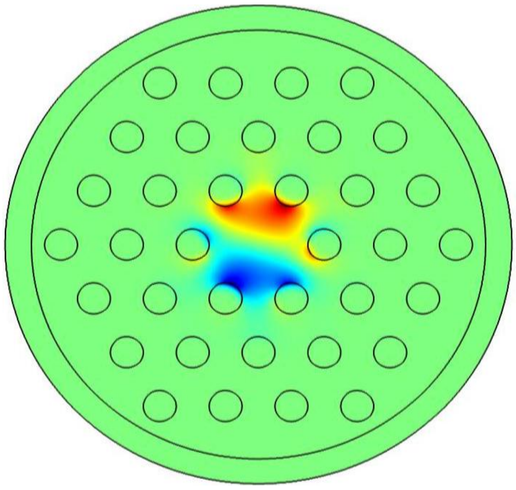

(b) Ez for Λ=5$\boldsymbol{\mu m}$

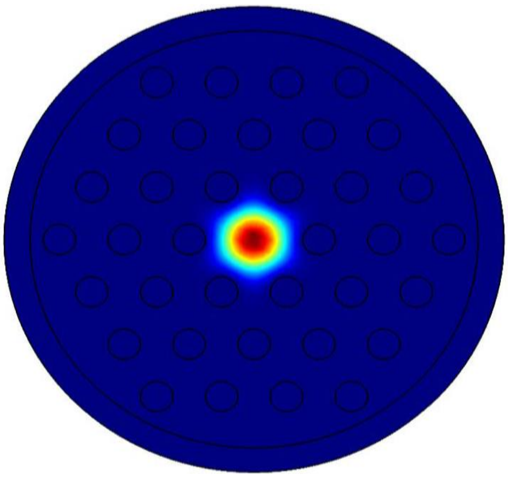

(c)Pz for Λ=5$\boldsymbol{\mu m}$

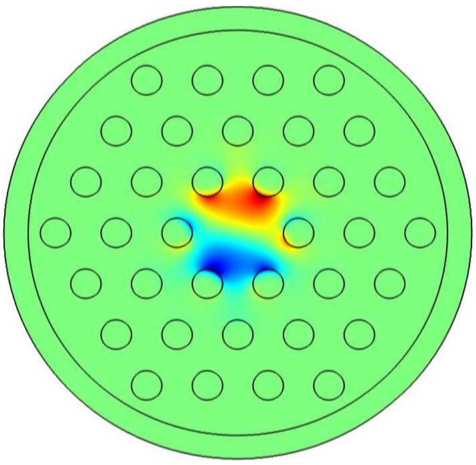

(d) Ez for Λ=5$\boldsymbol{\mu m}$

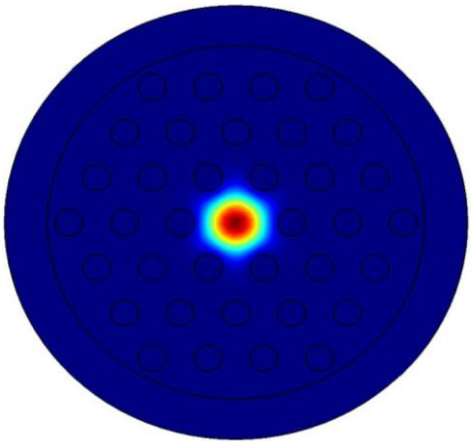

(e) Pz for Λ=2.6μm

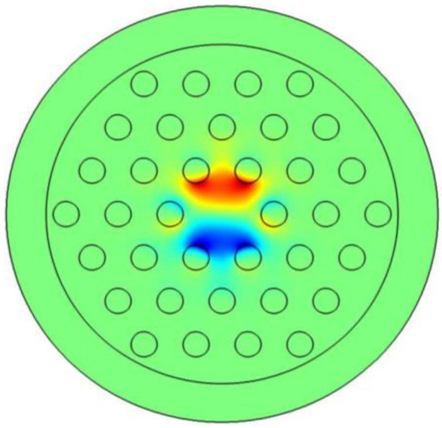

(f) Ez for Λ=2.6$\boldsymbol{\mu m}$

Fig 5.5: The field distribution and effective area of H-PCF.

5.1.9 Bending Loss

As mentioned earlier the bending loss occurs in the PCF due to bending of the fiber. To determine this bending loss PCFs of 3 pitch has been simulated in COMSOL 4.4. During this simulation the refractive index is always kept as equation 5.1. By using this refractive index fiber is simulated for different values of R. From this simulation effective index is found. To understand the concept of bending loss properly first we need to realize the modal shift of PCF due to bending. Electric field distribution for different bending radius at 1.55μm has been given in fig.5.6. Fig.5.6 depicts that the modal field shifts towards cladding as bending radius is decreased. The bending tolerance of PCF of pitch 1.6 is higher than other PCFs. That means the bending tolerance of low pitch PCF is higher than the high pitch PCF.

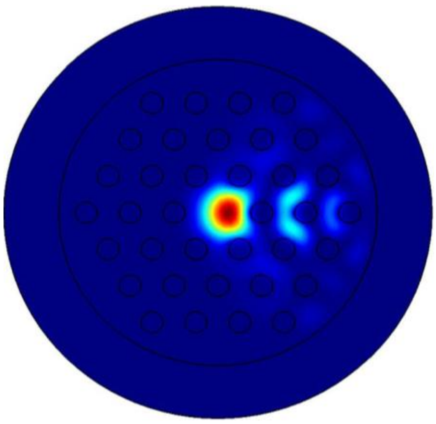

(a)Bending radius50μm forΛ=1.6μm

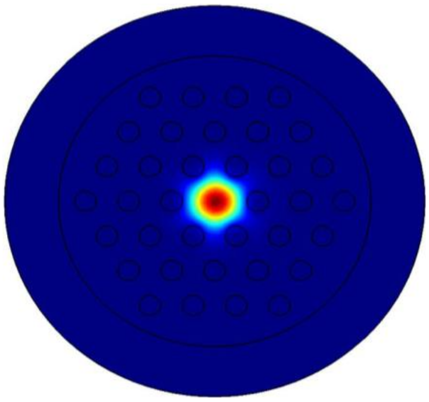

(b) Bending radius 500μm forΛ=1.6μm

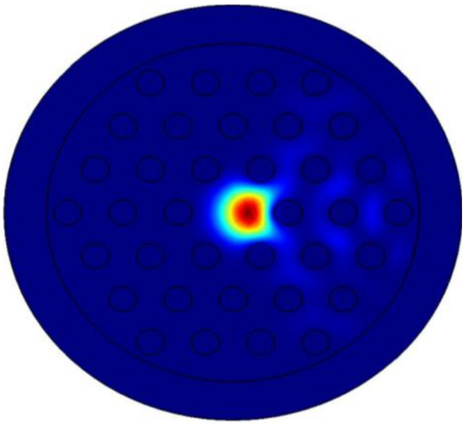

(c)Bending radius 150μm for Λ=2.6μm

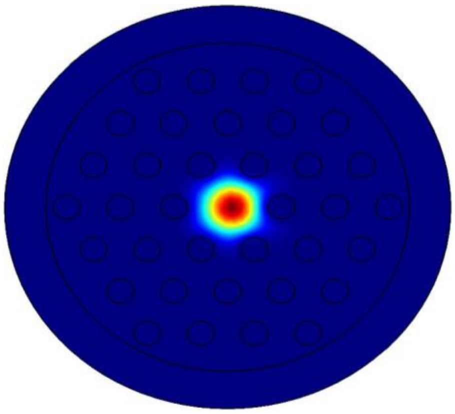

(d)Bending radius 50μm for Λ=2.6μm

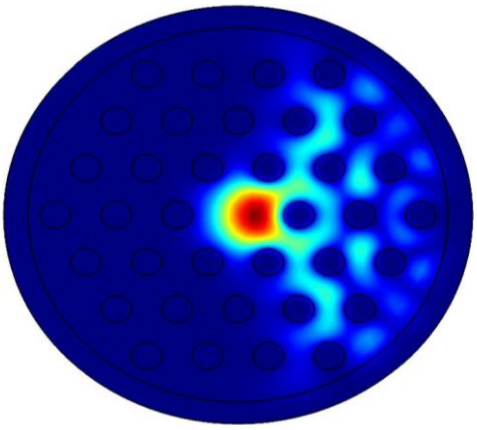

(e) Bending radius 850$\boldsymbol{\mu m}$ for Λ=5$\boldsymbol{\mu m}$

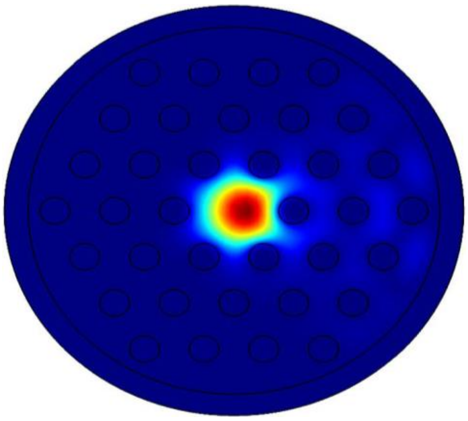

(f) Bending radius 1350$\boldsymbol{\mu m}$ for Λ=5$\boldsymbol{\mu m}$

Fig.5.6: Electric field distribution for different bending radius of H-PCF.

By this way simulation for varying R has been done for each PCF. After this simulation by using the imaginary part of effective index, bending loss is determined. The bending loss has been determined for both fundamental modes. The result has been compared with the result of a reference. The result has been given in the Fig 5.7a.

From Fig. 5.7a it is obvious to us that, for a lower pitch length of 1.6μm, the bending loss increases monotonically as the bending radius is reduced. It can tolerate high bending. But in this case bending loss is higher. For low pitch leakage loss which is also called confinement loss is also high as the PCF is operating close to its modal cutoff. In large bending radius the loss gets saturated. This loss is confinement loss or leakage loss. So using a PCF with such a smaller pitch length is often not preferred due to its higher leakage losses. As the pitch length is increased, for 2.6μm the leakage loss is reduced by

3 orders of magnitude as expected. The bending loss is also lower after a certain radius. Beyond this radius, as the bending radius is reduced, the bending loss increases progressively and as a result the total loss also increases. It can be noted that the increase in the bending loss with the bending radius are more rapid as the bending radius is reduced, compared to the case with a lower pitch length of 1.6μm. At a lower bending radius, the non-monotonic nature is also seen with oscillations in the total loss values. When the pitch length is increased further, for pitch length of 5 μm the leakage loss is significantly reduced to 10^{-3}dB/m and a PCF with a larger dimension is often then preferred. But, in this case the PCF is more susceptible to bending, and the total loss value increases rapidly as the bending radius is reduced. It also cannot tolerate too much bending. For some fixed radii, this value can even be higher than that of a PCF with a lower pitch value. Again, in this case of a larger Λ, the oscillations in the loss values are more frequent and appear to be random in nature.

We know that any PCF has two fundamental modes. The bending loss for another fundamental mode has been determined. The comparison of these two modes has been given in figure 5.7b. From figure 5.7b we can say the modal and leakage properties of both the modes are almost similar and also located at similar locations. Due to this loss in two modes are close to each other.

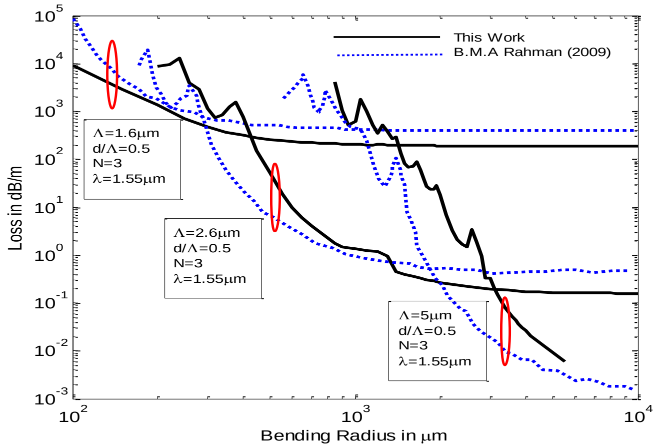

Fig.5.7a: Bending Loss vs. Bending Radius

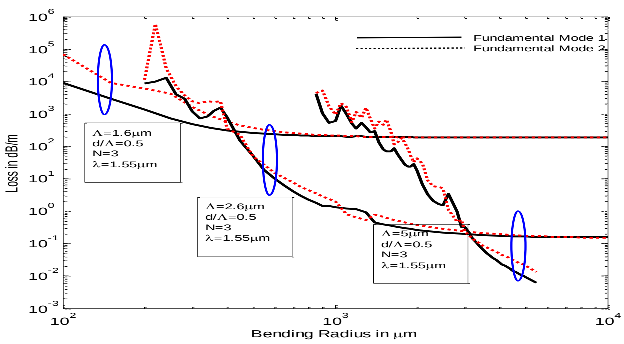

Fig. 5.7 b: Bending loss vs. bending radius for two modes

5.1.10 Confinement Loss

It is well known that normally PCF suffers from leakage loss as the modal index is lower than the refractive index of the outer cladding silica region. This leakage loss is called confinement loss. This confinement loss occurs when the fiber is in straight condition no bending or bending radius is too high. In case of the determination of variation of confinement loss with respect to wavelength, we need to consider the Selmer equation as stated above because due to the change of wavelength change in refractive index of silica occurs. To include this effect the Selmer equation has been used as refractive index of silica. So, when the simulation is varied for different wavelength refractive index automatically vary and finally we get correct result. To understand the concept of confinement loss properly first we need to realize the modal shift of PCF due to wavelength.

To determine the confinement losses, PCF of these three pitches has been simulated by varying wavelength. After simulation effective refractive index for fundamental mode has been found. By using the imaginary part of this effective index, we can easily determine the confinement loss or leakage loss for any fiber.

We have done all these simulations by sweeping wavelength we have determined effective index for each pitch. Then by using the above-mentioned formula we have determined confinement loss vs. wavelength graph for different values of pitch. As stated earlier there are two fundamental modes in PCF. So, confinement losses have been calculated for both modes. Then graph is generated by MATLAB which depicts the variation of confinement losses with respect to wavelength for given pitch and mode. This graph has been shown Fig. 5.8. In Fig. 5.8 it proves the previous statement that small pitch can tolerate small wavelength while large pitch can tolerate large wavelength. The confinement loss is too small in large pitch PCF than in small pitch PCF. Because in a large pitch PCF the air hole diameter increased as d/Λ is fixed at 5. So, the relative fraction of air is increased as a result the confinement loss is decreased. As confinement loss for both modes is very close to each other we can easily say that modal and leakage properties of both the modes are almost similar.

5.1.11 Effective Area

Effective area is first of all an important quantity in the context of nonlinearities, but it also has connections to leakage loss, macro-bending loss, and numerical aperture. We have determined the effective area, A_{eff} of hexagonal index guided PCFs of different pitch value. We used electric field distribution as field to determine effective area. To determine the effective area in COMSOL, at first simulation is executed and fundamental mode is detected. Then integration over total surface is done for $(abs(normE))^2$ and $(\mathrm{abs}(\mathrm{normE}))^4$. Now the square of the first result is divided by the second integration result. This result is effective area as previous formula suggest. By this way we easily can determine the relationship of effective area with wavelength and bending radius.

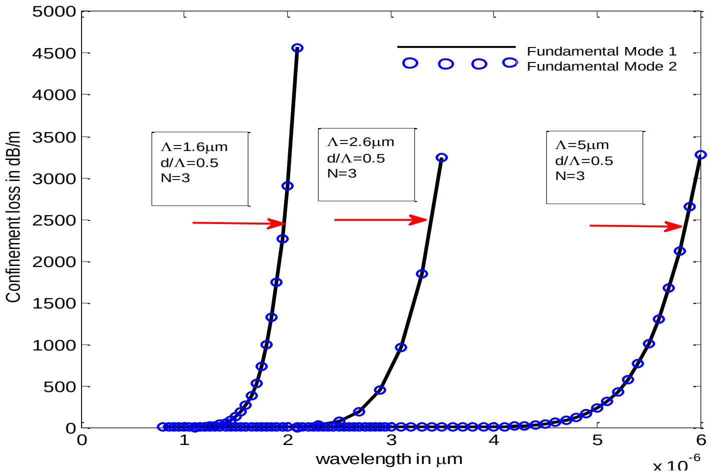

Fig. 5.8: Confinement loss vs. wavelength

To determine this relationship simulation of determining Confinement loss has been used. By surface integration in COMSOL $(abs(normE))^2$ and (abs(normE)) ^{4} has been determined. The effective area increases with wavelength. The effective area is large for higher pitch and small for lower pitch. It also depicts that low pitch PCF can tolerate small amount of wavelength while large pitch fiber can tolerate large PCF. Like bending and confinement loss, effective area for both modes is very close to each other. So we can easily say that modal and leakage properties of both the modes are almost similar.

5.1.12 Dispersion

The phenomenon of spreading a short pulse of light is called chromatic dispersion. We know that this chromatic dispersion, D in [ps/(nm.km)], of a PCFs can easily be calculated**.** To determine this relationship simulation of determining confinement loss has been used. By using the real part of effective index dispersion has been calculated for different wavelength. Then by using MATLAB we have plotted this with respect to wavelength for different value of pitch. These results have been plotted in Fig. 5.9. The relation between wavelength and dispersion is random for each PCF.

We used finite element method (FEM) in COMSOL Multiphysics 4.4 to simulate different results of a thesis. We varied different parameters of the proposed square lattice photonic crystal fiber to get the desired result.

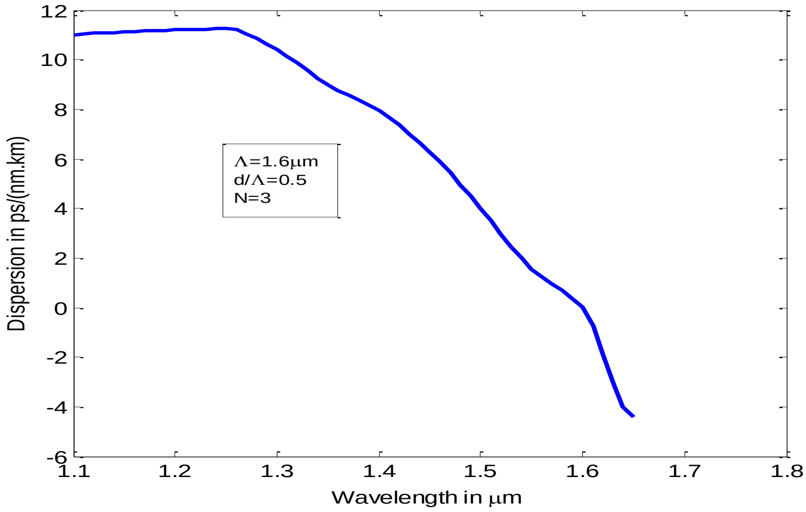

Fig. 5.9: Dispersion at $\Lambda=1.6\boldsymbol{\mu m}$

5.2 Rectangular Lattice PCF(R-PCF)

R-PCF means rectangular PCF. That is the shape of the PCF is rectangular. The range of frequency of this PCF is in communication bands.

5.2.1Rectangular Lattice PCF Structure

We analyzed the square lattice photonic crystal fiber with the innermost ring of smaller diameter air hole.

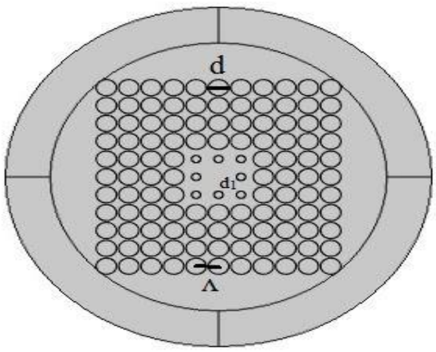

Fig 5.10: Schematic cross-section of the modified index-guiding SPCF with five rings of air holes. Smaller air hole diameter d_1 is for the two inner rings and larger diameter d for the outer four rings.

In the Fig. 5.10, we have the schematic cross section of the square lattice PCF with five rings, which is composed of circular air holes in the cladding arranged in a square array, where , Λ is the center-to-center spacing between the air holes (pitch), d is the bigger air hole diameter corresponding to cladding, d_1 is the smaller air hole diameter nearest to the core and d/Λ is the normalized diameter of air holes in the cladding .In this design, there is three degrees of freedom: 1st ring diameter, d_1, outer hole diameter d, air hole pitch Λ.

In conventional PCFs (air hole with same diameter in the cladding region), it is difficult to control dispersion and low confinement loss in a wide wavelength range. This is permitted for index-guiding PCFs as periodicity is not essential to guide the light in the core region based on the total internal reflection (TIR) mechanism.

5.2.2 Material filling

We used COMSOL 4.4 for the purpose of material filling. There are three types of geometric entity level in the structure which is to be filled with material: surface, circular holes, perfectly matched layer (PML).

In this structure, there are 125 individual domains in our COMSOL interface. Among them, 6-125 are circular holes filled with air, 1-4 are the PML domains filled with silica glass and the domain no.5 is also filled with silica glass.

Here, refractive index of the air is kept 1 which is independent of wavelength and refractive index of the silica is set according the Selmer equation, an empirical relationship between refractive index and wavelength for a particular transparent media.

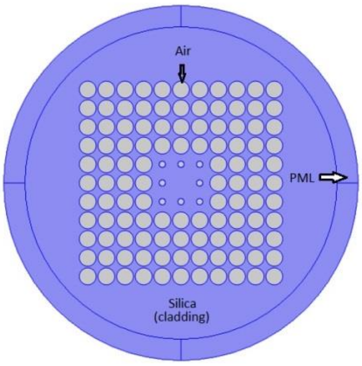

Fig. 5.11: Material filled square lattice PCF

The usual form of the equation for silica glasses is

$$n^2(\lambda) = 1 + \frac{B_1\lambda^2}{\lambda^2 - C_1} + \frac{B_2\lambda^2}{\lambda^2 - C_2} + \frac{B_3\lambda^2}{\lambda^2 - C_3} \tag{5.2}$$

where n is the refractive index, λ is the wavelength, and $B_{1,2,3}$ and $C_{1,2,3}$ are experimentally determined Selmer coefficients. These coefficients are usually quoted for λ in micrometers. Note that this λ is the vacuum wavelength.

5.2.3 Modal Analysis

We did frequency domain modal analysis after assigning desired study settings such as: mode analysis frequency, desired number of modes, search for modes around etc. to get the single mode in the fiber.

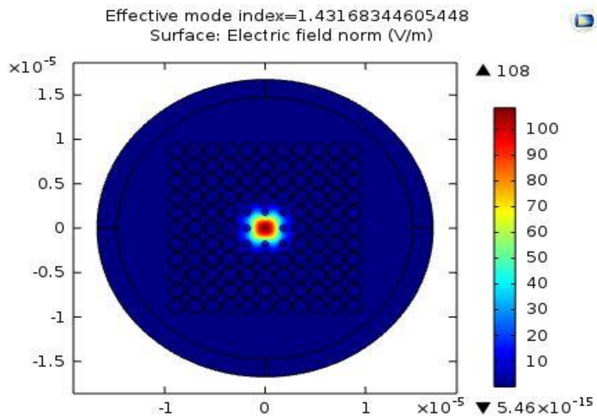

Fig. 5.12: Surface plot of the normalized electric field for eff. Mode index=1.431683 at wavelength=1.2[um]

Then we did the global evaluation from the COMSOL and derived the effective mode index for wavelength equally spacing from 1200[nm] to 2000[nm].

After getting the data from the global evaluation matrix, we implemented them with proper MATLAB code to obtain the desired dispersion curve. Here, by desired curve we meant the zero-flattened dispersion with huge bandwidth (BW). For the proposed structure above, wek tried to tailor the dispersion curve using two degrees of freedom independently. Firstly, we considered the normalized diameter of the innermost ring air hole array. By changing this parameter, we have managed to flatten the dispersion curve. Secondly, we tried to shift curve vertically by changing the pitch of air hole.

We started our dispersion tailoring with the concentration on diameter of the inner most ring air hole array. The figures obtained are displayed sequentially below.

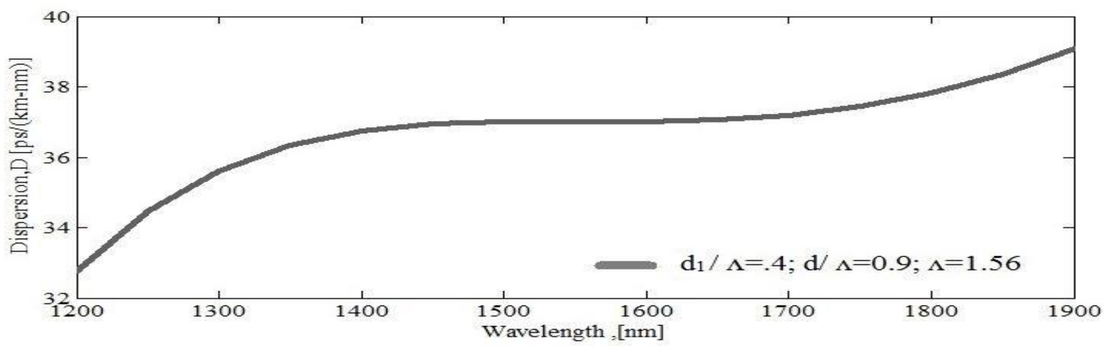

Fig 5.13: Dispersion behavior.

A normalized air-hole diameter of outer ring is chosen 0.9. Large normalized air-hole dimension is selected for better field confinement for the guided mode. Suitable normalized air-hole diameter of inner rings is found by calculating the dispersions as a function of wavelength. In general, these parameters will influence the slope behavior of the chromatic dispersion curves. In the figure above, we see that, the slope of the curve is changing from positive to negative with the increase in the normalized diameter of inner rings from 0.36 to 0.43.

We observed from the curve with d_1/Λ =0.36, slope of the curve remained zero for a huge BW of 300 nm. And it is called wavelength-flatted dispersion. So, we took this parameter granted as dispersion flattened. Now, our next move is towards curve shifting.

Effect of change in pitch of the air hole

In this second step, the final parameter, air-hole pitch, is varied to find our target that is zero chromatic dispersion in wide-band wavelength range. Fig. 5.14 shows the effect of changing from 1.46 to 1.66 um on the chromatic dispersion behavior with d/Λ =.9 and d_1/Λ =.4. It is obviously seen that the air-hole pitches dominantly influence the dispersion level but has a little effect on the slope of the dispersion. The dispersion level is about 31.5, 37, and 41ps/km/nm, respectively, for Λ =1.46, 1.56 and 1.66[um]. Although the dispersion level is varied, the wavelength-flattened behavior is not changed for different Λ.

Though air-hole pitch can dominantly influence the dispersion level, we observed in the Fig.5.15 that huge decrease in the air hole pitch gives us a zero crossing but changes the wavelength-flatted shape. So, here comes the importance of a modification in the structure.

Below curve of dispersion, confinement loss, effective area and nonlinearity are shown for Λ=1.00[um]; d_1/Λ=.40; d/Λ=.90 in the figure 5.14.

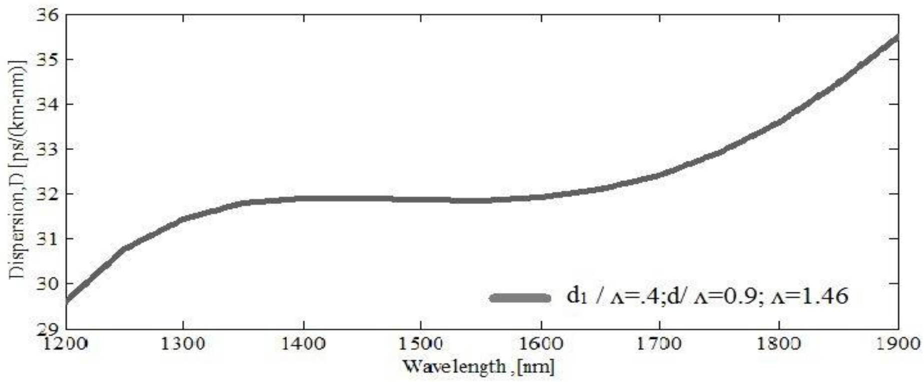

(a)

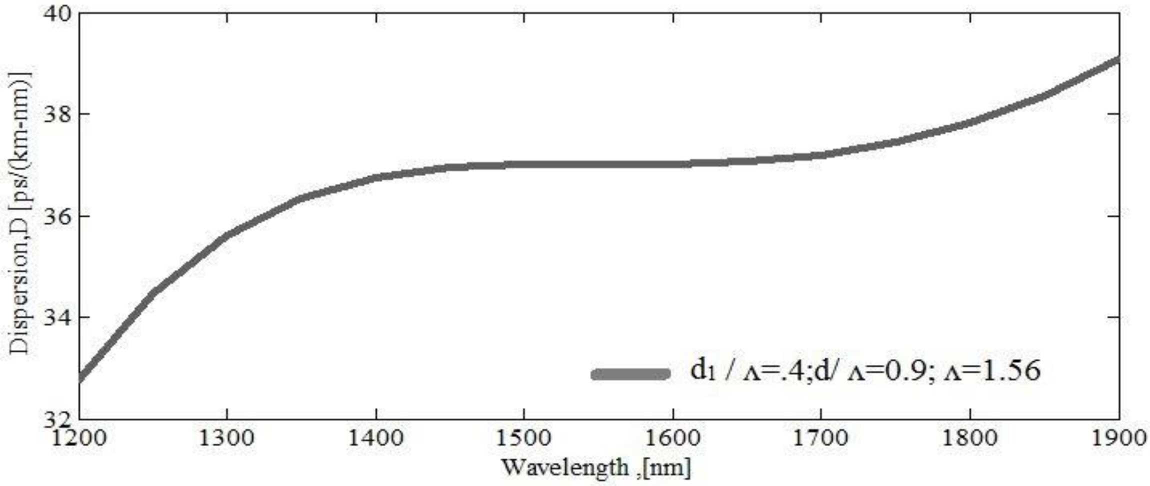

(b)

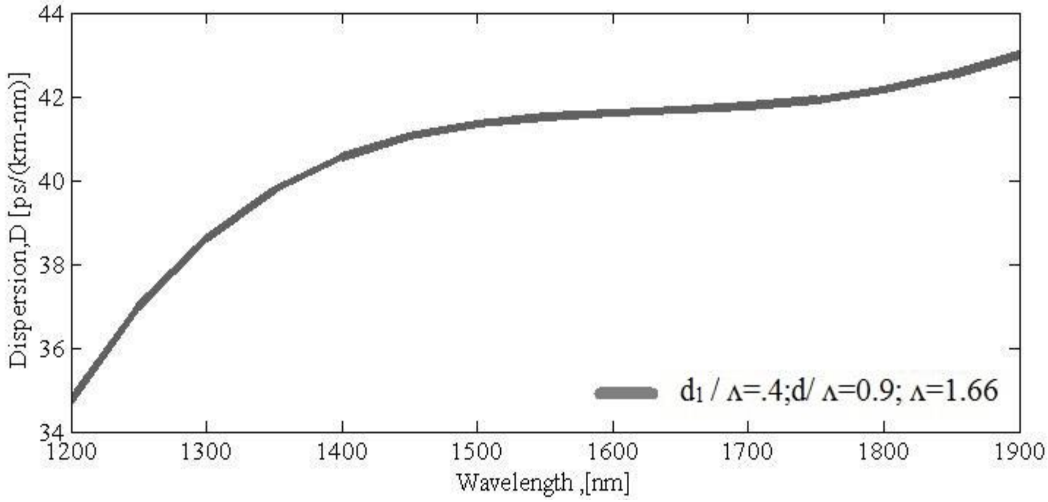

(c)

Fig. 5.14: Effect of **Λ** on Dispersion behavior for (a) 1.46[um]; (b) 1.56[um]; (c) 1.66[um] at d/A=.9 and d_1/**Λ**=.4

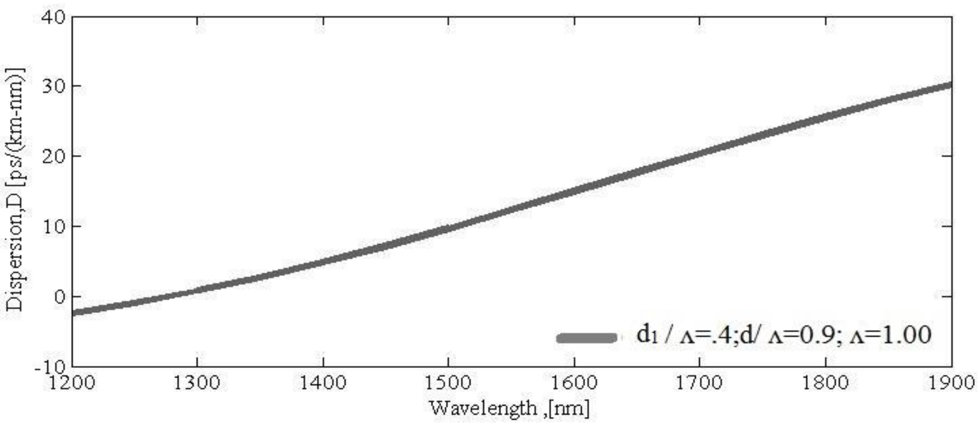

(a)

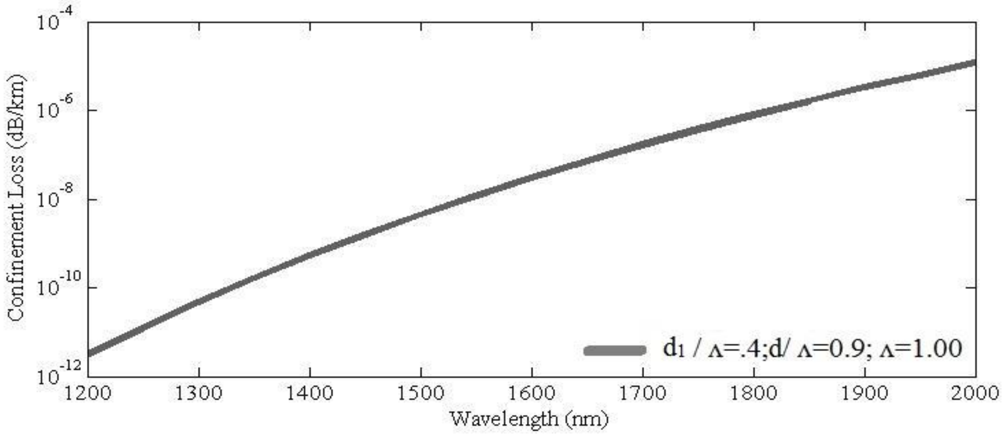

(b)

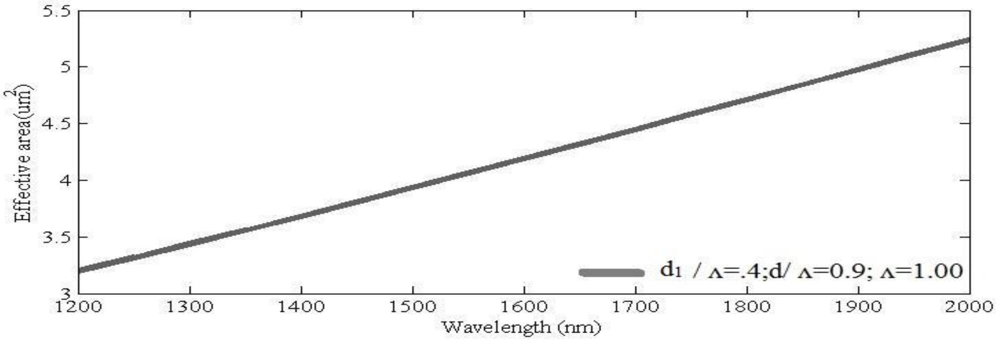

(c)

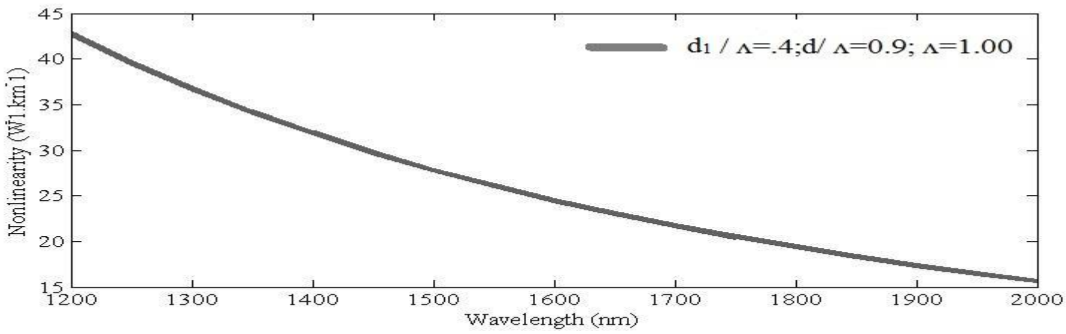

(d)

Fig. 5.15: (a) dispersion;(b) confinement loss;(c) effective area;(d) nonlinearity curve for $d_1/\Lambda=0.4$; d/A=0.9and A=1.00[um]

5.3 THz PCF

Normally in our thesis we have researched vigorously about the THz PCF. That is the PCF with frequencies in terahertz range. The structure we have normally discussed is hexagonal. The hexagonal structure normally gives the idea of the analysis and different characteristics properties of PCF. There can be other structures too like octagonal and decagonal which will show the similar properties as the hexagonal PCF. So here we have considered hexagonal PCF as our ideal case.

5.3.1 ADVANTAGES OF TERAHETZ RADIATION

Signatures of several bio-chemical species are carried by the terahertz (THz) regime and are thus important for applications such as imaging, non-destructive testing and detection of complex compounds. Probes in the terahertz regime are used for sensing of drugs/explosives/weapons in a non-destructive manner that could be vital in security and defense, detecting and understanding the dynamics of complex biological systems. However, a flexible low loss THz waveguide is useful for delivery from source to sensor or double up as the sensor.

Recently photonic crystal fibers (PCF) have also been demonstrated for terahertz guidance. Material loss, confinement and bending losses of the waveguide along with dispersion, birefringence and single/multi-mode behavior of the guides have been crucial in determining performance and practical use. This led to the development of several terahertz sources including several different guides. Waveguides includes polymer PCF. The latter often utilize a ‘drill and draw’ or ‘stack and fuse’ technology for fabricating fibers. An ideal fiber like PCF is easy and cheap to fabricate, have very low loss, flexible, appropriately tailored dispersion and single moded.

We present a hexagonal design inspired by nature for PCF in the Terahertz regime. This PCF has hexagonal ultra-low bending loss and lower confinement losses. A vectorial finite element method has been used for the rigorous analysis of the fibers.

WHY RESEARCHERS DECIDED TO USE THIS GAP

This frequency range can transfer huge data files via wireless route and can significantly increase the communication data rate over existing microwave technology. THz waves can deeply penetrate through cloths, ceramics, walls, woods, paper, dry air, polymers etc., but they are absorbed or reflected by metal, water vapor, dust, cloud, and sufficiently dense objects. Additionally, THz waves are also not harmful to human health. All these excellent qualities of THz radiation make it suitable for imaging of hidden objects, like explosives, metallic weapons etc. Most importantly, this technology has already begun to make deep inroads in non-invasive medical diagnostics, such as detection of skin cancer, tooth decay, and identification of human tissues based on different refractive indices and linear absorption coefficients at THz frequencies.

5.3.2 STRUCTURE

Below shows the simple structure of our terahertz PCF where the parameters are shown clearly. We have obtained our fundamental mode at 1THz frequency and thus the wavelength is 255.14um.

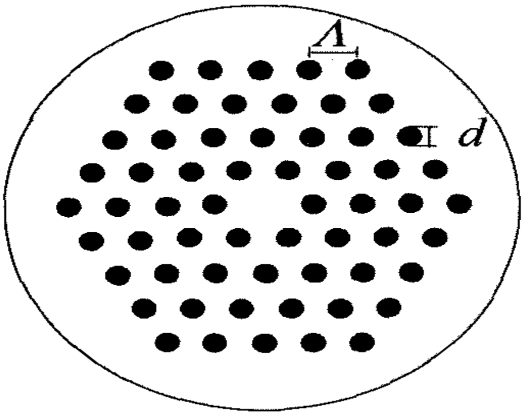

Fig. 5.16: Simple Structure of THz PCF.

PARAMETERS:

The main parameters are diameter of holes, period, wavelength and frequency which are described briefly below.

Parameters

Name	Expression	Value
p	500[um]	5.0000E-4 m
d	.4*p	2.0000E-4 m
wavelength	255.14[um]	2.5514E-4 m
freq	c_const/wavelength	1.1750E12 1/s

Table 5.1: Parameters of THz PCF

We have used the diameter as 500um [1]. Each of the holes is made of air. We know the refractive index of air is 1. We have used 59 air holes in our structure in which all the structure of air holes are circular. We have used array method to make the sequential arrangement of holes in a hexagonal way which gives our hexagonal structure.

Here we have used the ratio 0.4 as a standard parameter in our structure. We can also use 0.8 and 0.6. In every case we will obtain the same profile and the entire characteristics graph will be same.

There a Perfectly Matched Layer (PML) surrounding the cladding domain as shown in Fig. 5.17, to absorb the radiating mode. The wavelength of the PML must correspond to the radial wave vector component for the wave [9]. We have used this layer known as PML in our structure, which gives our structure protection from the outside world. The PML layer is made of the same material as the surface and it is given in four layers. For a PCF giving of PML layer is very important. If PML layer is not given then there are difficulties with the structure also and we cannot get the correct structure.

MATERIAL

We have used two materials in our structure which are described as follows

1. **POLYETHYLENE**
   The material we have used at the surface is made up of polyethylene. Its refractive index is 1.5628
2. **AIR HOLES**
   The air holes are circular and made up of air. Its refractive index is 1. There are 59 air holes, all of the same size and are in hexagonal structure.

We have drawn the structure. How are we going to determine whether the structure is correct or not. We can understand the structure is correct when the light passes through the core of the structure in different electric and magnetic fields at the fundamental mode. We can understand this more accurately by observing different graphs.

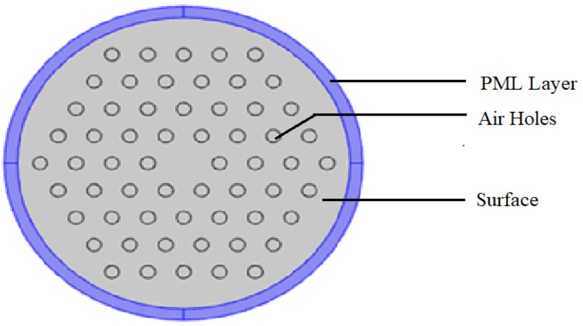

Fig 5.17: PCF structure showing PML layer, air holes and surface.

Surface electric energy density time average graph:

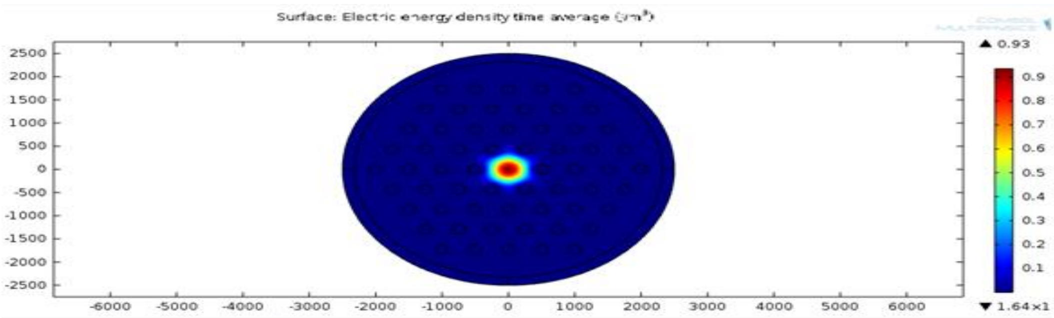

Fig. 5.18: Surface energy density time average graph

Power flow x component:

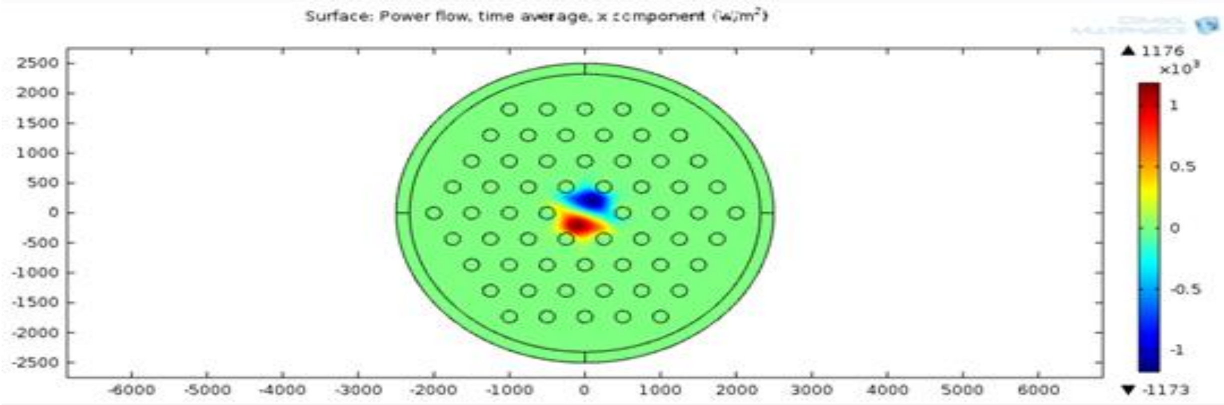

Fig. 5.19: Surface power flow, time average, x component

Power flow y component:

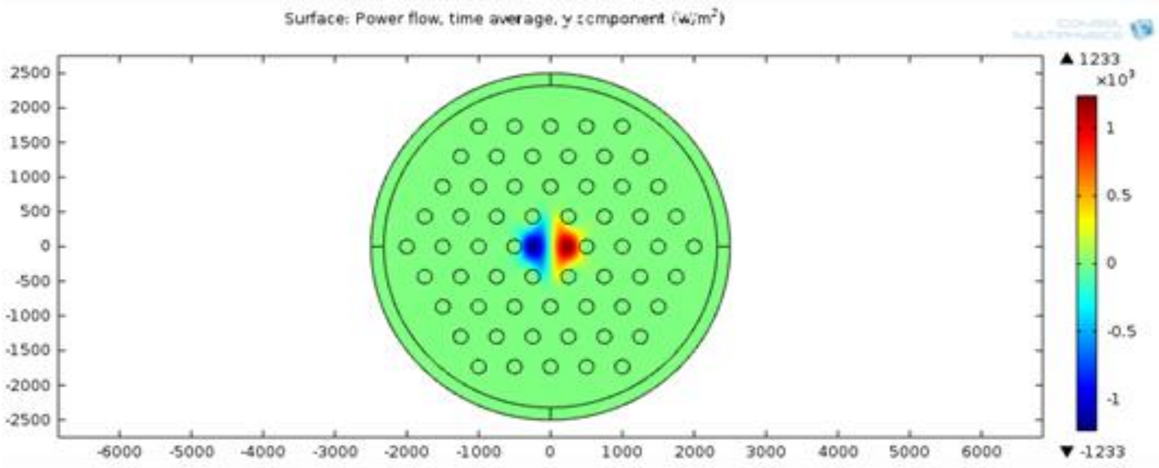

Fig. 5.20: Surface power flow, time average, y component

Power flow z component:

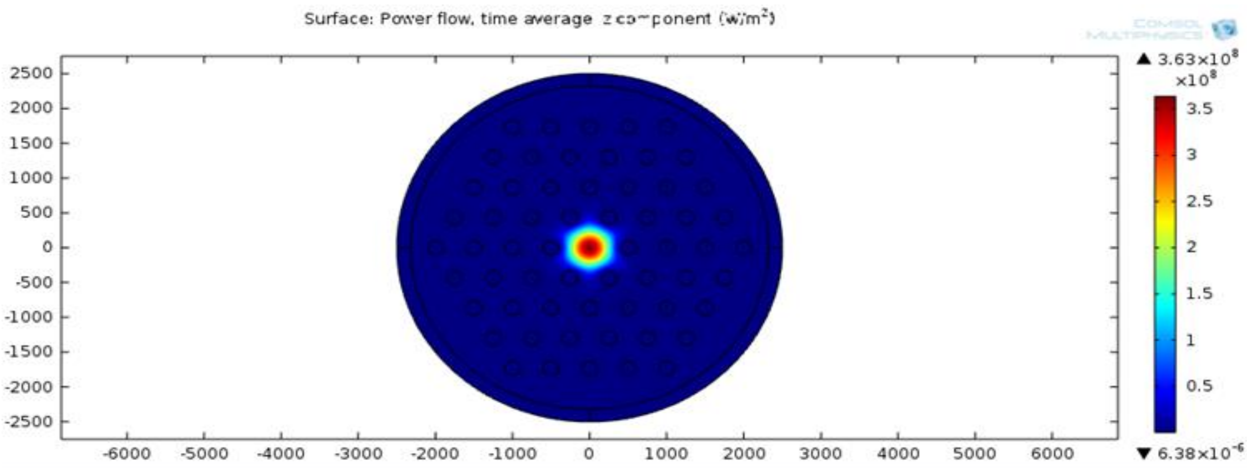

Fig. 5.21: Surface power flow, time average, z component.

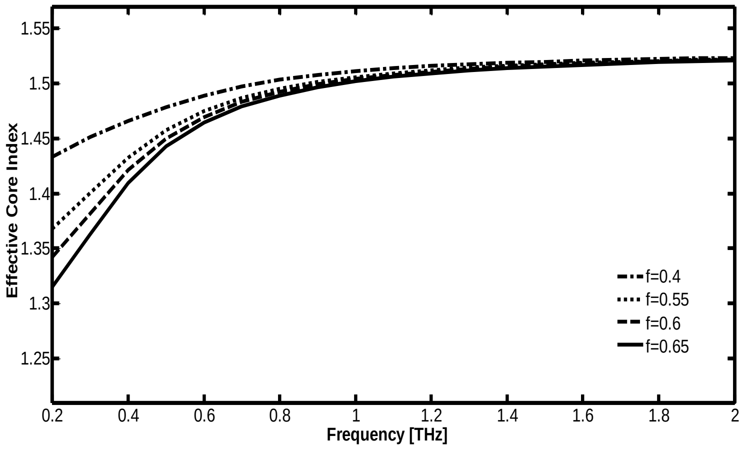

Fig. 5.22**:** Effective Core Index vs. Frequency

:

In Fig. 5.22, we have obtained a non-linear curve increasing rapidly from the low frequencies and in the center or fundamental core frequency which is 1 we obtain a steady response and later on with high frequency we have obtained a little rapid change. This is a non-linear proportionate curve. In the end of the response the change becomes steady at about effective index 1.55.

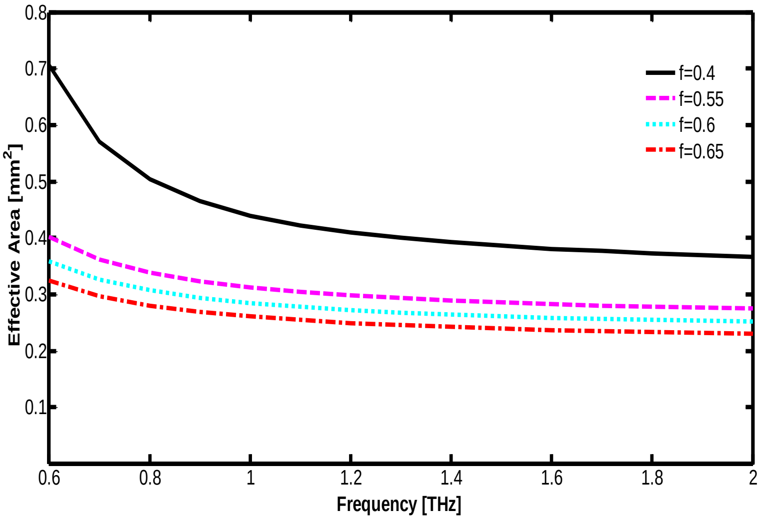

Fig. 5.23: Effective Area as a function of frequency

Fig. 5.23 shows the effective area profile of terahertz photonic crystal fiber against frequency. In the graph we can see that at first when the frequency is low then the effective mode index is high then when the frequency increases then gradually the effective mode index decreases rapidly then after the fundamental mode at high frequencies there is no rapid decrease of effective index. The effective index becomes steady. So, the curve is a non-linear curve generally which changes rapidly or the slope is high at the beginning and then gradually the response becomes steady at about effective area of 0.4.

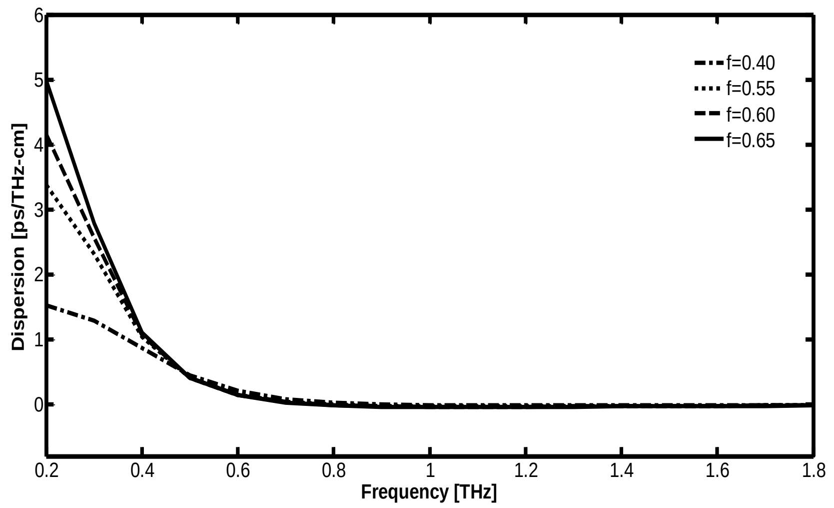

Fig. 5.24: Dispersion as a function of frequency for various filling factor

Here Fig. 5.24 shows for different values of d/A with dark and dashed lines. The above figure shows the dispersion profile of terahertz photonic crystal fiber against frequency. In the graph we can see that at first when the frequency is low then the effective mode index is high then when the frequency increases then gradually the effective mode index decreases rapidly then after the fundamental mode at high frequencies there is no rapid decrease of effective index. The effective index becomes steady. So, the curve is a non-linear curve generally which changes rapidly or the slope is high at the beginning and then gradually the response becomes steady at about dispersion 0. We have obtained zero or flattened dispersion graph.

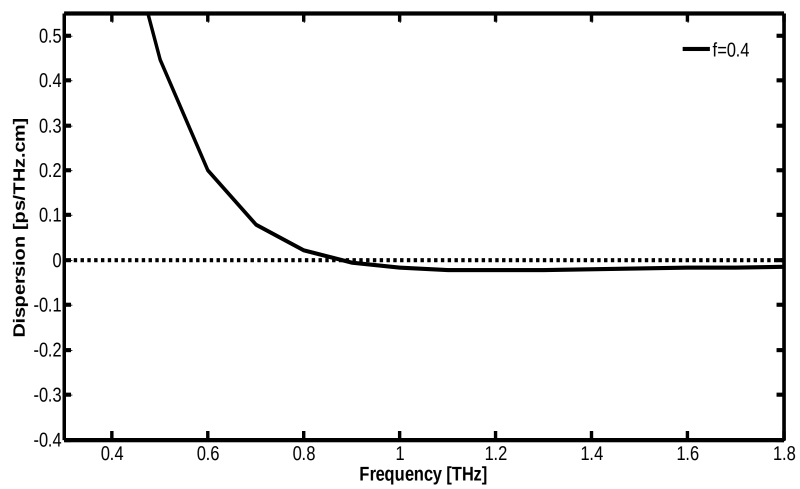

Fig. 5.25: Dispersion profile for the THz PCF with Λ=500 µm and d/Λ=0.4

Here Fig. 5.25 shows for d/A=0.4. The above figure shows the dispersion profile of terahertz photonic crystal fiber against frequency. In the graph we can see that at first when the frequency is low then the effective mode index is high then when the frequency increases then gradually the effective mode index decreases rapidly then after the fundamental mode at high frequencies there is no rapid decrease of effective index. The effective index becomes steady. So, the curve is a non-linear curve generally which changes rapidly or the slope is high at the beginning and then gradually the response becomes steady at about dispersion 0. We have obtained zero or flattened dispersion graph.

CHAPTER 6

CONCLUSION

In summary we have investigated the dependence of the single mode condition and dispersion property for the plastic triangular THz PCF on the structure parameter d/p. When d/p is less than 0.475, then the THz PCF supports a single mode below 2.5 THz. We saw that the dispersion profile becomes flattened as d/p decreases. The dispersion coefficient is considered -0.03+.02 or -0.03-.02 ps/THz when p=500um and d/p=0.4. The single mode THz PCF can be used in the construction of compact THz devices and also in measurement systems.

6.1 Conclusion of the work

An immensely lower effective material loss, notably marginal core power fraction, less confinement loss and near zero ultra-flat dispersion has been introduced in our proposed design. In our proposed design, single mode properties has also been satisfied and designed for THz wave guidance. Our proposed design contains attractive guiding properties which will be significant for THz wave application. For long distance communication of THz signal, our proposed design can be used relevantly.

Despite of its youth in the sensing field, PCFs have awakened the interest of many scientific groups due to their promising characteristics. The biggest attraction in PCFs is that by varying the size and location of the cladding holes and/or the core the fiber transmission spectrum, mode shape, nonlinearity, dispersion, air filling fraction and birefringence, among others, can be tuned to reach values that are not achievable with conventional OFs. Additionally, the existence of air holes gives the possibility of light propagation in air, or alternatively provides the ability to insert liquids/gases into the air holes. This enables a well-controlled interaction between light and sample leading to new sensing applications that could not ever be considered with standard OFs. Due to PCFs diversity of features they introduce a large number of new and improved applications in the fiber optic sensing domain.

The main drawback of our proposed design is power fraction can further be increased. PCFs reflect light only within a certain frequency range whereas metals reflect all light. So, a PCF cavity can have only one mode rather than the infinity of modes of a metal cavity that endanger beam stability when excited by the beam. It may even be possible to operate PCF waveguides and cavities in a chosen mode of higher order.

6.2 Future Scope

Our proposed PCF architecture is significantly simpler than other structures proposed so far for controlling the chromatic dispersion and at the same time ultra-flattened dispersion characteristics have been obtained over a wide frequency range. Additionally our proposed PCF architecture shows low confinement losses as well as small effective mode area, which are novel properties in an ultra-flattened dispersion design. The main conclusion of this systematic approach is that with a modest number of design parameters we could fully-tune and optimize the chromatic dispersion properties of the PCF. Our architecture is suitable for applications as a chromatic dispersion controller, dispersion compensator and if we can get a lower effective area by further modifying this design then we can get a highly nonlinear PCF leading to supercontinuum generation.

REFERENCE

[1] Frederic Zolla, Gilles Renversez, Andre Nicolet, Doris Kuhlmey, Sebastian Guennea, and Didier Felbecq, "Foundations of Photonic Crystal Fibre", Imperial College Press, 2005.

[2] Anders Bjarkleb, Jes Broeng, and Araceli Sanchez Bjarklev, "Photonic Crystal Fibre", Kluwer Academic Publishers, 2003.

[3] Knight, J. C., "Photonic crystal fibers," Nature, vol. 424, pp. 847–851, 2003.

[4] Russell, P. St. J., "Photonic crystal fibers," Science, vol. 299, pp. 358–362, Jan. 2003.

[5] M. D. Nielsen, C. Jacobsen, N. A. Mortensen, J. R. Folkenberg, and H.R.Simonsen,"Low-loss photonic crystalfibersfor transmission system and their dispersion properties, " Opt. Expr., vol. 12, pp. 1372 –1376, 2004.

[6] L. P. Shen, W. P. Huang, and S. S. Jian, "Design and optimization of photonic crystal fibers for broad-band dispersion compensation," IEEE Photon. Technol. Lett. , vol. 15, no. 4, pp. 540 –542, Apr. 2003.

[7] V. Finazzi, T. M. Monro, and D. J. Richardson, "Small-core silica holey fibers: Nonlinearity and confinement loss tradeoffs," J. Opt. Soc. Amer. B, vol. 20, pp. 1427 –1436, 2003.

[8] Mortensen, N. A., Folkenberg, J. R., Nielsen, M. D., and Hansen, K. P., "Modal cutoff and the V parameter in photonic crystal fibers," Optics Letters, vol. 28, pp. 1879–1881, 2003.

[9] de Matos, C. J. S., Taylor, J. R., Hansen, T. P., Hansen, K. P., and Broeng, J., "All-fiber chirped pulse amplification using highly-dispersive air-core photonic bandgap fiber," Optics Express, vol. 11, pp. 2832–2837, 2003.

[10] Limpert, J., Schreiber, T., Nolte, S., Zellmer, H., and Tunnermann, A., "All fiber chirped-pulse amplification system based on compression in air guiding photonic bandgap fiber," Optics Express, vol. 11, pp. 3332–3337, Dec. 2003.

[11] de Matos, C. J. S. and Taylor, J. R., "Chirped pulse Raman amplification with compression in air-core photonic bandgap fiber," Optics Express, vol. 13, pp. 2828–2834, Apr. 2005.

[12] Humbert, G., Knight, J. C., Bouwmans, G., Russell, P. St. J., Williams, D. P., Roberts, P. J., and Mangan, B. J., “Hollow core photonic crystal fibers for beam delivery,” Optics Express, vol. 12, pp. 1477–1484, Apr. 2004.

[13] J. Ju, W. Jin, Senior Member, IEEE, and M. S. Demokan, Senior Member, IEEE, “Properties of Highly Birefringent Photonic Crystal Fiber”, IEEE Photonics Technology Letters, Vol. 15, No. 10, October 2003.

[14] W.H. Reeves, J.C. Knight, P.St.J. Russell and P.J. Roberts, “Demonstration of ultra-flattened dispersion in photonic crystal fibers”, OPTICS EXPRESS 613, Vol. 10, No. 14, 15 July 2002.

[15] Latest developments in Photonic Crystal Fiber, “ www.youtube.com”, August 3, 2015.

[16] Arismar Cerqueira S. Jr., F. Luan, C. M. B. Cordeiro, A. K. George and J. C. Knight, “Hybrid photonic cry stal fiber”, OPTICS EXPRESS 92623, Vol. 14, No. 2 , January 2006.

[17] Gelin Zhang, Fengfei Xing, Peiguang Yan, Huifeng Wei, Huiquan Li, Shisheng Huang, Rongyong Lin and Kangkang Chen, “Double Cladding Seven- core Photonic Crystal Fiber”, Optics and Photonics Journal, 2013, pp 47- 49.

[18] Shizhuo Yin and Ruyan Guo, “Advances in Materials and Innovations in Device Applications VIII ”, SPIE Proceedings, Vol.9200, September 5, 2014.

[19] T.S. Sainia, A. Bailib, A. Kumara, R. Cherifb, M. Zghalb and R.K. Sinhaa, “Design and analysis of equiangular spiral photonic crystal fiber for mid-infrared supercontinuum generation”, Journal of Modern Optics, Volume 62, Issue 19, pages 1570- 1576, June 9,2015.

[20] C. Martelli, J. Canning, M. Kristensen, and N. Groothoff, “Refractive index measurement within a photonic crystal fibre based on short wavelength diffraction,” Sensors, vol. 7, no. 11, pp. 2492–2498, 2007.

[21] Y. Zhu, Z. He, and H. Du, “Detection of external refractive index change with high sensitivity using long-period gratings in photonic crystal fiber,” Sensors and Actuators B, vol. 131, no. 1, pp. 265–269, 2008.

[22] Nafiz Amin and Mohammad Faisal, “Highly nonlinear polarization-maintaining photonic crystal fiber with nanoscale GaP strips”, vol. 55, No. 35, pp. 10030-10036, December 10, 2016.

[23] Raonaqual Islam, Sohel Rana, Redwan Ahmad, and Shubi Felix Kaijage, “Bend-Insensitive and Low-Loss Porous Core Spiral Terahertz Fiber.”, vol. 27, No. 21, pp. 2242-2245, November 1, 2015.

[24] Raonaqual Islam, Md. Selim Habib, G. K. M. Hasanuzzaman, Redwan Ahmad, Sohel Rana, and Shubu Felix Kaijage, “Extremely High-Birefringent Asymmetric Slotted-Core Photonic Crystal Fiber in THz Regine.”, vol. 27, No. 21, pp. 2222-2225, November 1, 2015.

[25] Alwyn J. Seeds, Fellow, IEEE, Haymen Shams, Member, IEEE, Martym J. Fice, Member, IEEE, and Cyril C. Renaud, Member, IEEE, “TeraHertz Photonics for Wireless Communications.”, vol. 33, No. 3, pp. 579-587, February 1, 2015.